Hardware improvement in cold pressor test and Peltier system for measurement of hemodynamic response to pain by fNIR Spectroscopy

A Thesis

Submitted to the Faculty

Of

Drexel University

By

Rutvi Vyas

In partial fulfillment of the

requirements for the degree

of

Master of Science in Biomedical Engineering

August 2012

© Copyright 2012
Rutvi Vyas. All Rights Reserved.

ACKNOWLEDGEMENTS

I would like to thank all the people involved in this project through their constant guidance, help and support. Firstly, I would like to express my gratitude towards my advisor, Dr. Kambiz Pourrezaei for his valuable guidance and encouragement to achieve success in my career.

I would also like to convey my sincere thanks to Dr. Meltem Izzetoglu, Dr. Hasan Ayaz and Dr. Arye Rosen for their guidance and feedback for my work, and to Dr. Onaral for providing me with this opportunity. My special thanks go to Ms. Zeinab Barati for her great help and contribution towards the research.

Grateful thanks also goes to my colleagues in the Optical Brain Imaging team, without whose help completion of this work would not have been possible. I would also like convey my gratitude to Mr. Bruno Pechhiura for his contribution towards the project.

Last but not least, I would like to thank all my friends and family for their constant love, encouragement and support, which was essential for the accomplishment of this work.

TABLE OF CONTENTS

LIST OF FIGURES

LIST OF TABLES

ABSTRACT

Hardware improvement in cold pressor test and Peltier system for measurement of hemodynamic response to pain by fNIR Spectroscopy

Rutvi Vyas

Advisor: Dr. Kambiz Pourrezaei

Functional Near-Infrared (fNIR) spectroscopy is a relatively new imaging technology which allows a continuous and non-invasive monitoring of changes in cerebral hemodynamics and blood oxygenation. A number of studies have reported changes in the hemodynamic activity in response to experimental pain in human subjects using several imaging modalities, including fMRI and laser Doppler sonography/flowmetry. In our lab (CONQUER CollabOrative, Drexel University) fNIR is employed to study the changes in hemodynamic responses to acute cold pain.

The hemodynamic response to different levels of pain has been investigated at our lab by delivering cold noxious stimuli by limb immersion in cold water a.ka. cold pressor test (CPT) and through ceramic plates (Peltier device) respectively. Two configurations of 'far' and 'near' optode spacing were used to investigate both pain-related cortical as well as systemic hemodynamic changes. However, the existing sensor used for capturing the fNIR recording needed some further hardware improvement to eliminate the glitches in smooth experimentation. Moreover, there was a critical need for developing corresponding adapter circuit for the control circuit used for operating the

light sources and photo-detectors of the fNIR sensors. Furthermore, optimum parameters to be used for delivering cold noxious stimuli needed to be investigated for the existing peltier device setup. This thesis addresses these hardware designs and development concerns done to achieve better experimentation. Results from tolerance tests using CPT suggest that the systemic change in the blood flow in response to acute episodes of cold painful stimuli can be objectively monitored and assessed through the biological marker measured by fNIR spetroscopy. Results from Peltier study suggest that noxious cold stimuli evoke a less generalized hemodynamic response when compared with CPTs, which is yet detectable with fNIR spectroscopy.

CHAPTER 1: INTRODUCTION

Pain is one of the most common reasons for patients to seek medical attention and one of the most prevalent medical complaints [1]. It is defined by IASP (International Association for the Study of Pain) as "An unpleasant sensory and emotional experience associated with actual or potential tissue damage, or described in terms of such damage" [2]. Despite many people suffering from chronic pain, the field of pain management is not very advanced, partly due to lack of a reliable tool for objective assessment of pain. A recent market research states that more than 1.5 billion people worldwide suffer from chronic pain of varying degrees and about 3-4.5% of the global population suffers from neuropathic pain [3]. According to American Academy of Pain Management, the number of chronic pain sufferers outweighs other major health conditions like diabetes, heart disease and cancer combined. A lot of money, ranging from $560 billion to $635 billion (in 2010 dollars), is spent on healthcare due to pain annually in the United States [4]. This clearly indicates the need of objective assessment of pain even though pain is considered subjective. It would be very useful for clinicians to have the ability to objectively monitor and evaluate pain from a robust biomarker.

Studies have been done to measure hemodynamic response in individuals [5-8]. Previous studies of brain responses to pain stimuli have been done using different modalities including fMRI (functional Magnetic Resonance Imaging), Laser Doppler sonography/flowmetry and PET (Positron Emission Tomography) [9-18]. These studies

have shown relations between pain stimulus intensity, patient rating of the pain, and activations of certain brain areas. All these modalities have been greatly useful in enhancing our knowledge about the physiological changes in the brain as well studying the neural circuits. However, each of these techniques has its own shortcomings. fMRI poses restrictions to the subject as it is sensitive to motion artifacts and exposes them to loud noise and discomfort. It is very expensive and difficult to establish in a clinical setup [19]. Single point laser Doppler delivers poor spatial resolution as opposed to fMRI and is also sensitive to motion artifacts, whereas laser Doppler imaging equipment has better spatial resolution but poor temporal resolution and is very expensive [20]. On the other hand, PET requires injection of radioactive material and also has a claustrophobic setup like fMRI causing discomfort to the subject [19]. These limitations thus give rise to the need of a feasible, inexpensive, portable, non-invasive and reliable tool for objective assessment of pain. fNIR spectroscopy has been introduced as a new neuroimaging technique which enables real-time measurement of hemodynamics and tissue oxygenation non-invasively [21, 22]. It also permits several benefits like easy operation with high time resolution and adequate spatial resolution for continuous recording of [HbO_2] and [Hb] changes of brain, non-ionizing radiation imaging, and compact implementation, long time monitoring and low cost [23]. Thus fNIR spectroscopy has been employed at our lab as a potential imaging technique for pain assessment.

In order to study the hemodynamic response to pain in humans, induction of experimental thermal pain has been used. Two of the major techniques widely used for inducing experimental cold noxious stimuli have been cold pressor tests and use of a Peltier thermode. The hemodynamic response to different levels of pain, have been investigated at our lab by delivering cold noxious stimuli by limb immersion in cold water (cold pressor test) and through ceramic plates (Peltier device) respectively.

PROBLEM STATEMENT

In order to investigate the response to pain through fNIR spectroscopy, certain problems in the hardware needed to be resolved within the system:

1) *Multi-distance configuration of probes:* In the design of fNIR sensors, which consists of infrared light source and photodetectors to capture the hemodynamic response, a multi-distance source-detector configuration was used. Two different distances, 1 cm and 2.8 cm, were employed. The near detector which was positioned too close to the photodetector, would get saturated, resulting in collection of non-reliable data. Also, the gain of the detector could not be controlled over the individual channels which resulted in a change of overall gain for the system instead of a particular channel.
2) *Adapter for the control unit:* The control box of the fNIR system was developed for a commercially available fNIR sensor. This sensor consisted of 16 channels which detected hemodynamic response from 16 different locations while up to 8 channels were needed in the pain experiments. The custom sensor developed for pain experiments needed to be used with an already existing acquisition unit. As a result,

the control box could not be directly used for taking measurements from the fNIR system.

3) *Optimization of Parameters:* In order to use the existing Peltier set up for delivering thermal noxious stimuli, there was a need to determine appropriate values of temperature on the hot as well as the cold side to generate a detectable hemodynamic response while simultaneously accounting for human safety. This required estimation of an appropriate balance between two parameters: the minimum and maximum temperature of the Peltier surface for the delivery of cold and hot stimulus respectively, and the rate of change of this temperature with respect to a baseline (adaptation) temperature.

These problems needed to be addressed in order to proceed towards experimentation.

SOLUTIONS

1) To address the first issue of saturation of near channel, the circuit diagram of the photodetector was studied and a resistance was added across the detector to reduce its voltage sensitivity and hence the gain of near channel detector could be adjusted.
2) A solution to the second problem was to design the right adapter tailored for the fNIRS sensors used in pain experiments. An adapter circuit was fabricated to deliver power from the supply source to reach the appropriate LEDs and photo-detectors.
3) In case of the Peltier setup, various tests were performed including changing the amount of current supplied to the Peltier device, varying the baseline (adaptation)

temperature as well as the water bath temperature to control the minimum and maximum safe limit of temperature for delivering noxious stimuli as well to avoid overheating of the device. This paved a way for determining the optimum parameters for using the Peltier device to conduct experiments.

The above mentioned solutions played a major role in simplification of the experimental procedures resulting in better acquisition of the data through the fNIR system. It also helped in increasing the feasibility of the apparatus and aided in better comprehension of concepts behind the working of fNIR spectroscopy. Moreover, the process of optimizing various parameters for use of the Peltier setup, helped in understanding the characteristics and working of Peltier device at a great depth and hence deciding the usability of the device as a means to deliver experimental thermal stimuli. Thus, the improvements and modifications of the hardware and experimental protocol paved the way towards successful experimentation of using fNIR spectroscopy with cold pressor tests and Peltier device system.

In a nutshell, the following goals could be defined for this work:

An IRB for performing cold pressor tolerance test was to be obtained. A protocol was to be developed and an IRB to conduct cold experiments using Peltier device was to be obtained. One of the goals of this work was also to debug and modify all the necessary hardware to carry out the cold pressor tests and the cold experiments using Peltier device. Another aim was to obtain pilot data to demonstrate that both systems and

protocols are calibrated, validated and are ready for the above IRB approved clinical trials.

This thesis talks about the hardware development and improvement done in the apparatus and protocol for using two modalities: CPTs and Peltier device; for inducing experimental pain in human subjects and monitoring the response through fNIR spectroscopy. The principle, experimental setup and the results obtained from the pilot studies done after the improvement have also been discussed to give an insight about the success of these modifications.

CHAPTER 2: FUNCTIONAL NEAR-INFRARED SPECTROSCOPY – BASICS AND ITS APPLICATION IN PAIN STUDY

This chapter discourses the basic principle of functional near-infrared spectroscopy and how this principle has been exploited to be used as an imaging modality for its application in pain study. During the course of this application for our research, certain hardware problems were encountered which have been discussed along with the solutions employed.

2.1 BACKGROUND

2.1.1 PRINCIPLES

Absorption of light by hemoglobin is strong in the visible range but decreases significantly in the near infrared range, while its absorption by water increases beyond wavelength of 900 nm [24-34]. Thus biological tissues are relatively transparent to light in the near-infrared range between 700-900 nm (Figure 1) [35]. Even though there is a strong scattering of light by tissue, the radiation can be efficiently transmitted through skin and soft tissue over long distances, which makes this wavelength range an 'optical window' for non-invasive assessment of brain tissue [35, 36]. This light then gets absorbed by the chromophore, hemoglobin. There is a change in the absorption of the near-infrared light by these chromophores based on the change in their oxygenation states and this serves as the main principle of fNIR spectroscopy [37]. fNIR spectroscopy system consists of infrared source and detectors that receive light post-reflection.

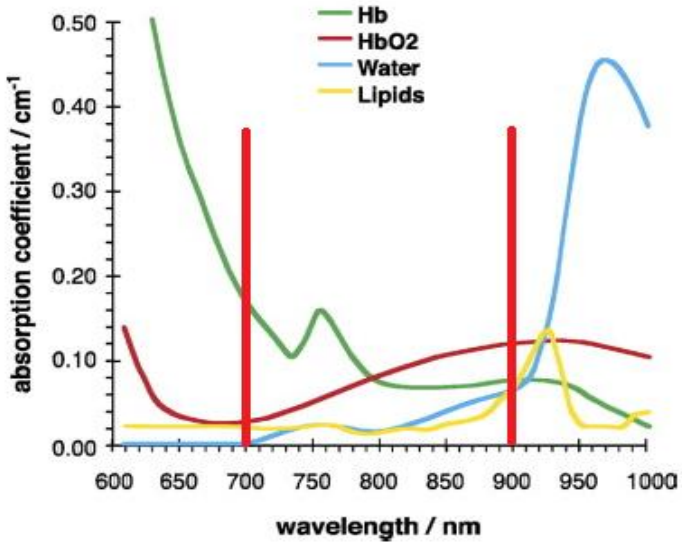

Figure 1: 'Optical Window' of biological tissue: Main tissue constituents absorbing in the 700–900 nm spectral range [38-49]

The photons emitted from the light source that enter the tissue undergo absorption and scattering and thus get attenuated. They easily pass through most of the tissues but reflect back from oxy- and deoxy-Hb [19]. fNIR spectroscopy measures this attenuation of light at different wavelengths in the near-infrared region where the changes in optical densities are attributed to changes in chromophore concentration in the illuminated volume on the basis of a modified Beer-Lambert's Law [50]. These fNIR spectroscopy measurements are carried out by reflection mode in which the infrared light travels in a shallow banana-shaped arc with a penetration depth of approximately half the distance between the source and the detector (Figure 2).

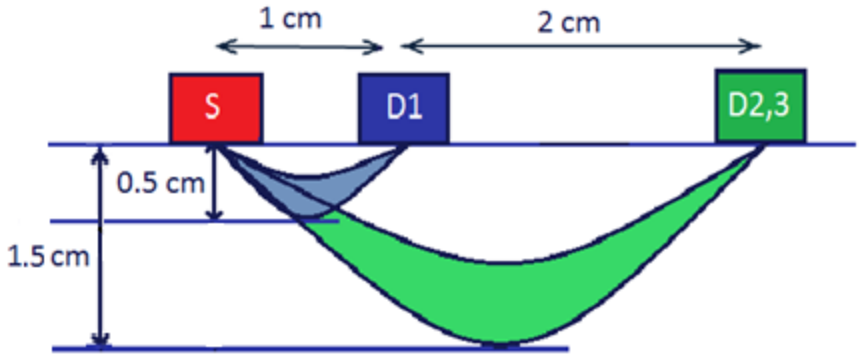

Figure 2: Banana-shaped pathway of infrared light in biological tissue

The equation for the modified Beer-Lambert Law is:

$$I = GI_0 * e^{-I(\alpha_{Hb}C_{Hb} + \alpha_{HbO2}C_{HbO2})}$$

G = factor that accounts for the measurement geometry and is assumed constant when concentration changes

I_0 = the input's light intensity

α_{Hb} and α_{HbO2} = the molar extinction coefficients of deoxyhemoglobin and oxyhemoglobin

C_{Hb} and C_{HbO2} = the concentrations of these chromophores

L = photon path which is a function of absorption and scattering coefficients (μ_a and μ_b)

If the intensity measurement at an initial time is Ib, and at another time is I, the OD (Optical Density) changes due to variation in C_{Hb} and C_{HbO2} during that period is calculated as:

$$\Delta OD = log\ (Ib/I) = \alpha_{Hb}\, C_{Hb} + \alpha_{HbO2}\, C_{HbO2}$$

By measuring optical density (OD) changes at two wavelengths, the relative change of Hb and HbO_2 versus time can be obtained. Change in oxygenation and blood volume or total hemoglobin can then be calculated as:

$$\text{Oxygenation} = \Delta C_{HbO2} - \Delta C_{Hb}$$

$$\text{Blood Volume} = \Delta C_{HbO2} + \Delta C_{Hb}$$

2.1.2 PAIN RESEARCH USING fNIR SPECTROSCOPY

Several researches have been done to study the activity in the brain in response to pain. Induction of experimental hot and cold pain has been used widely for studying activation of various parts of brain. Thermal pain-evoked activity has been seen within the frontal lobe regions like anterior cingulate cortex as well as in secondary somatosensory, and primary somatosensory cortices during perception of painful heat stimuli [18]. Similar other studies have shown multiple representations of pain in the human brain. Casey et al. have studied the forebrain and brain stem structures that are active during perception of acute heat pain in humans in response to repetitive noxious thermal stimuli [9]. Coghill et al. have also studied changes in blood flow in the brain resulting as a response to painful thermal stimuli delivered to the forearm of human subjects [11]. Severe, localized cold stimulus is also known to elicit highly specific autonomic activity [51].

These changes in the brain are associated with changes in the optical properties of the outermost layer of brain tissue which can be measured by functional optical imaging. Functional optical imaging is the assessment of physiological changes associated with brain activity by means of optical methods [35]. Near-infrared spectroscopy can detect changes in the concentrations of oxy-hemoglobin ([HbO_2]) and deoxy-hemoglobin ([Hb]) in tissue based upon differential absorption at multiple wavelengths [5]. Villringer et al. have evaluated NIR spectroscopy as a tool for assessment of hemodynamic changes that occur during stimulation of brain function in human adults [8]. Now, increase in blood flow towards brain as a response to painful stimuli will lead to an increase in [HbO_2] and a decrease in [Hb] because more oxygenated than deoxygenated blood will fill the blood vessel. Such regional oxygenation surrounding brain has been measured by multichannel near-infrared spectroscopy in infants as well as in patients during cardiac surgeries [52, 53]. Thus fNIR spectroscopy has been employed by our lab for monitoring changes in hemodynamic response due to experimentally induced cold noxious stimuli.

2.2 HARDWARE DEVELOPMENT

Two main hardware issues were encountered during hardware development:

1) Saturation of near channel of the fNIR sensor
2) Excess channels in the control circuit

SATURATION OF NEAR CHANNEL OF THE fNIR SENSOR

In order to capture the hemodynamic response, as the first step in the fNIR system, a multi-distance configuration was used in the design of the probes, where two different distances: 1 cm and 2.8 cm, were used between the infrared light source (multi-wavelength light emitting diode manufactured by Epitex Inc. type L4*730/4*850 - 40Q96-I) and the photo-detector (OPT-101 manufactured by Burr-Brown Corporation)(Figure 3a and 3b). The LED comes in a STEM TO-5 package at 730 nm and 850 nm wavelengths with an output power of 5 to 15 mW. The photodetectors come in an 8-pin DIP package. The main reason to use two different distances between the source and the detectors was to allow the response to be captured at two different depths. In addition to this, the silicon used for the base of the probes increased their flexibility and reduced their weight. However, the near-channel would get saturated because of its close proximity to the LED source and the gain of the individual detectors could not be controlled. To avoid saturation, the near detector needed to be taped by leaving a pin-sized hole for allowing just a small amount of light to pass through (Figure 3c). This tape needed to be replaced before every trial as the dimensions of the holes were altered as a result of use and possible dirt accumulation which resulted in loss of productive time and consistent signal.

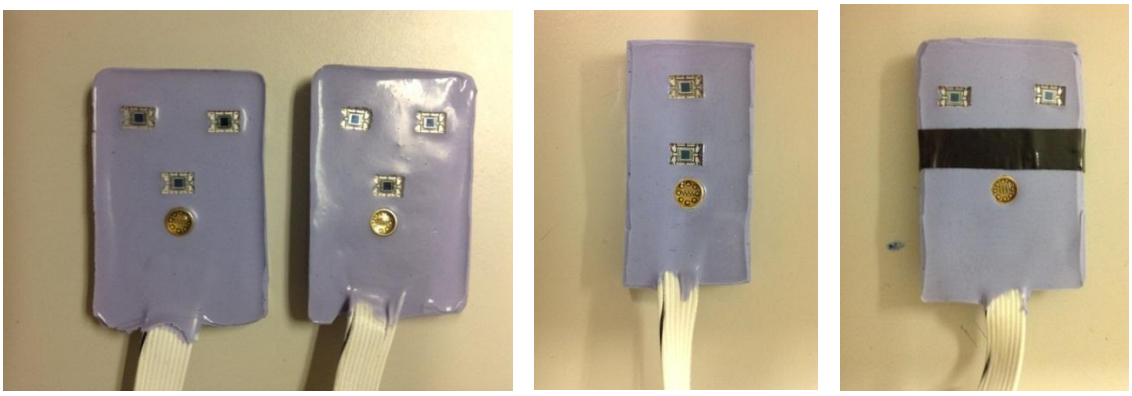

(a) (b) (c)

Figure 3: (a) Multi-distance probes; 1 source 3 detectors with S-D distance of 1cm and 2.8 cm
(b) Multi-distance probes; 1 source 2 detectors with S-D distance of 1cm and 2.8 cm
(c) Probe with a pin-size holed tape around near channel to avoid saturation

This problem could be eliminated if the gain of the near detector can be controlled individually. This was done by addition of an external resistance across the detector. This resulted in reduction in voltage sensitivity of the detector and hence decreased the gain of near channel detector. According to the datasheet for the photo-detector (Appendix A), an external resistor, R_{EXT}, can be connected to set a different voltage responsivity. A 1 M-ohm internal feedback resistance was provided in the photo-detector and thus to decrease voltage sensitivity, lower value of resistance, in the order of 10kOhm in this case, was applied across the detector to record a meaningful fNIR spectroscopy signal. This allowed individual control over the gain of the detector by controlling $R_{EXT.}$

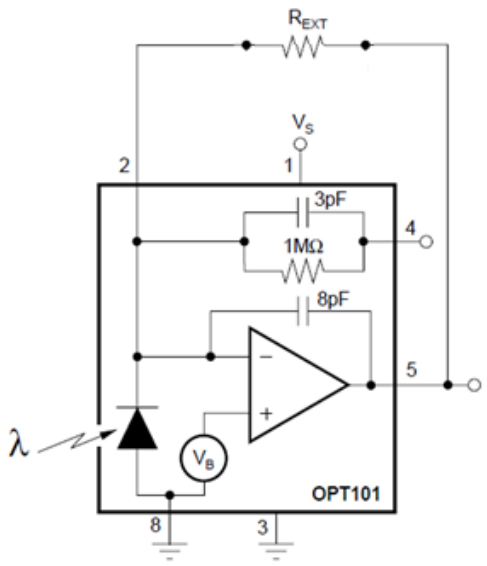

Figure 4: Changing responsivity of near photodetector with external resistor

EXCESS CHANNELS IN THE CONTROL CIRCUIT

Another obstacle in the path of smooth experimentation was that the control circuit used for operating the light sources and photo-detectors was designed to power the commercially available fNIR sensor which consists of 10 detectors and 4 LEDs. Each source-detector pair corresponds to a channel which in turn is displayed in each corresponding voxel. In the fNIR sensor shown in figure 6a, there are 4 sources and 10 detectors thus forming a total of 16 channels. These channels are displayed in corresponding voxels of the COBI Studio software which are shown in Figure 6b. Conversely, the fNIR sensors used in pain research consisted of 1 source and 3 detectors each (Figure 3a), resulting in 3 channels for each probe. Two such probes were used in pain experiments thus requiring 6 voxels corresponding to the 6 channels. Hence, the

configuration of the custom-made fNIR sensors used in pain research did not fit into the original design of the COBI Studio software. This resulted in excess channels showing a response in the COBI Studio software while there was an actual presence of only 6 channels. This gave rise to the need of an adapter for identifying the correct number of channels and eliminating any excess channels showing up on the software.

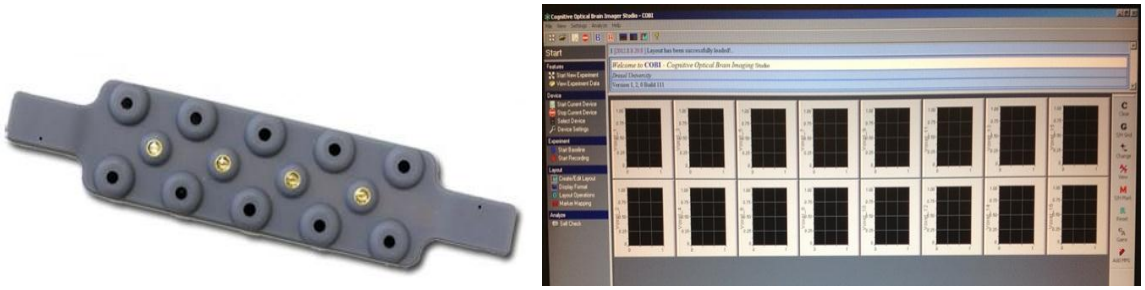

(a) (b)

Figure 5: (a) Commercially available fNIR sensor; 4 LEDs and 10 detectors (b) 16 voxels corresponding to 16 channels on the COBI software

In order to avoid this response from unwanted channels, a new adapter was designed as per the requirements of the number of channels. This adapter consisted of one 40-pin connector for communication with the control circuit and three 10-pin connectors for attachment of up to 3 probes. Two probes were to be used for pain experiments and an extra connector was provided so that a third probe (Figure 3b) could be attached to incorporate two more channels for future experiments. The connections available from the commercially available sensor were employed by using the required number of channels (Figure 6a and Appendix B). As shown in Figure 6b, the connections from the left-most and the right-most LEDs (LED-1 and LED-4) and their corresponding three

detectors (D1, D2, D3 and D8, D9, D10) were adapted for two of the new probe configurations as discussed previously. In addition to this, the connections from the LED-3 and its corresponding detectors (D5, D6) were adapted for an extra probe configuration with 1 source and 2 detectors (figure 3b) for future application. This design allowed appropriate recording of individual channels where voxels 1, 2 and 3 corresponded to channels of probe 1; voxels 14, 15 and 16 corresponded to channels of probe 2 and voxels 9 and 10 to channels of probe 3. This made the overall use of COBI software more feasible and appropriate for pain study.

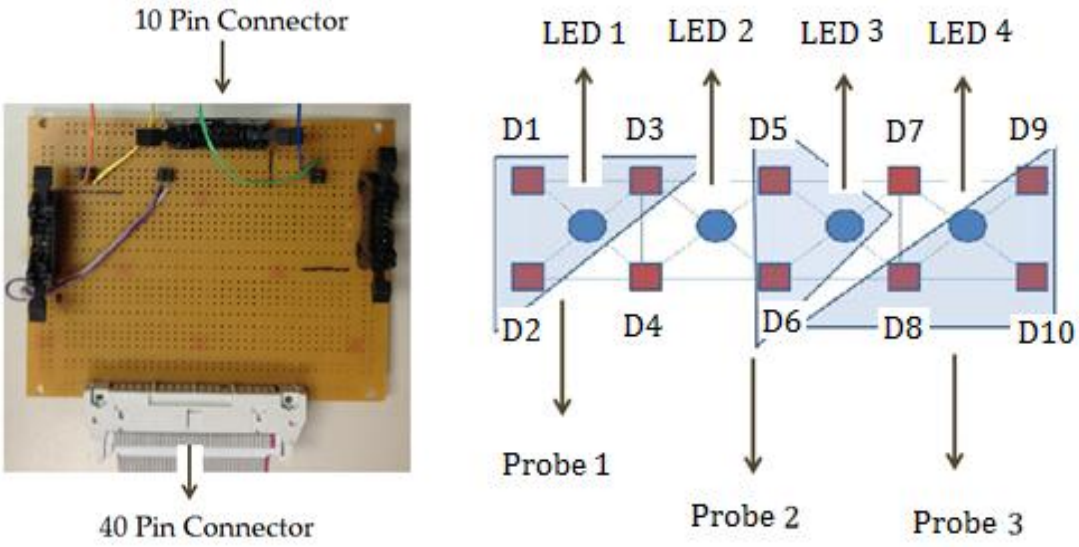

(a) **(b)**

Figure 6: (a) Adapter circuit for 3 probes: 40 pin connector for connection with the control circuit and 10 pin connectors for probe connection (b) Connections adapted from commercially available fNIR sensor

Investing time to tackle the hardware issues helped create reliable and efficient hardware, which were required to effectively continue with the tolerance tests using

cold water. The improved hardware as discussed in this chapter was then employed to run some successful cold pressor tests which are discussed in detail in the next section.

CHAPTER 3: COLD PRESSOR TESTS (CPT)

In this chapter, an overview of the use of CPT in the field of pain research has been discussed. The experimental setup section talks about the apparatus, protocol and procedure to run the tolerance tests using cold water followed by the results of the hemodynamic response evoked in the subjects due to the cold water stimulus. Thus the usability of the hardware, developed as discussed in chapter 2, has been presented.

3.1 LITERATURE REVIEW

Pain threshold and pain tolerance tests are used to find out the level at which pain begins to be felt and the maximum level of pain that a person is able to tolerate, respectively. These tests have proved to be very useful in learning about the physiological and psychological parameters in the human body. One of the techniques that have been widely used to determine the pain threshold and pain tolerance is the classic 'cold pressor test'; immersion of hand in ice-water. Several studies show that cold pressor test can be used successfully to evaluate psychological and physiological pain treatments and cold pressor tests have been used in fields like cardiovascular research since a long time ago [54]. Stocks et al. have shown a comprehensive overview of the human physiological responses to acute cold exposure [55]. The basis of their study was that the responses to cold, and the hazards associated with cold exposure, are moderated by factors which influence heat production and heat loss, including the severity and duration of cold stimuli, the magnitude of the metabolic response, and individual characteristics such as body composition, age, and gender. Furthermore,

Streff et al. have mentioned that the cold pressor test (CPT) is an empirically validated test commonly used in research on stress, pain and cardiovascular reactivity [56].

Wolf and Hardy used cold water at different temperatures ranging from -2^{o}C to 15^{o}C to study pain phenomenon due to local cooling [57]. They held their hand in cold water at 0^{o}C to 15^{o}C for as long as 10 minutes and at -2^{o}C for more than 4 minutes with no reported adverse effect. Streff et al. had performed the cold pressor test at 3-4°C with a cut-off predefined at 5 minutes [56]. Moreover, Walsh et al. had also used the temperature of water to be about 1-2°C [58]. Mitchell et al. performed the test at temperatures of 1°C, 3°C, 5°C, and 7°C and reported the tolerance limits as up to 150 seconds for 1°C and 3°C and up to 250 seconds for 5°C and 7°C in their population [59]. Based on such preliminary studies, we hypothesized that there is a relation between self-report of pain by the subjects during the threshold and tolerance tests and the measurements obtained by the fNIR spectroscopy. To test this hypothesis, we proposed using cold pressor test for the delivery of cold noxious stimuli. Given the above mentioned studies, we proposed the cut-off period of hand immersion in cold water as 5 minutes which could be considered as a safe duration for our experiments.

3.2 EXPERIMENTAL SETUP

3.2.1 APPARATUS

In order to collect the fNIR spectroscopy data, the continuous wave fNIR spectroscopy system, developed at Drexel University in our laboratory, was used. As described by Bahareh *et al.* it is composed of three sub-systems: (1) Two fNIR sensors with one light source and three photo-detectors each (2) A control circuit for operating the light sources and photo detectors (3) A software named COBI Studio developed in our laboratory at Drexel University for data acquisition and real-time data visualization. Two separation distances between the infrared light source and the photodetectors were used; 1 cm to monitor the absorption changes at the superficial layers while 2.8 cm for investigating deeper layers reaching the brain because the depth of penetration of near infrared light is half of the separation between source and detector.

The revised fNIR sensors were used to capture the response from the subjects. This modification of addition of external resistance proved to be advantageous in the experimentation. The duration of the pre-experimental setup time could be reduced to a great extent thus improving the quality of the testing. Moreover, the stability and consistency of the data were also affected positively. The newly fabricated adapter was used to bridge the second and third sub-systems of the fNIR spectroscopy system. The distinct assignment of channels aided in signal processing as well as data analysis.

For the delivery of cold noxious stimuli, constant temperature water bath (RM6 Lauda Brinkmann) was used and the temperature of this water bath was maintained at 5^{o}C. In

addition to this, a water bath, with water kept at room temperature (~23 ^{o}C), was used for generating a thermally neutral sensation for pre-stimulus recording.

3.2.2 PROTOCOL AND PROCEDURE

Two fNIR sensors of the same configuration as previously described were positioned symmetrically on the left and right sides of a subject's forehead proximate to the anterior median line and were secured using a medical band aid and a Velcro strap. Raw optical intensity measurements were collected at a sampling frequency of 2Hz in a dimly lit room with an ambient temperature of ~23^{o}C. The effect of background light on fNIR spectroscopy data was negligible and in fact, since the fNIR spectroscopy measures the relative changes in Hb and HbO_2 concentrations with respect to a baseline condition, this effect was washed out in the calculations. Subjects were seated comfortably in an armchair, facing away from the experimenter to minimize any distraction (Figure 7).

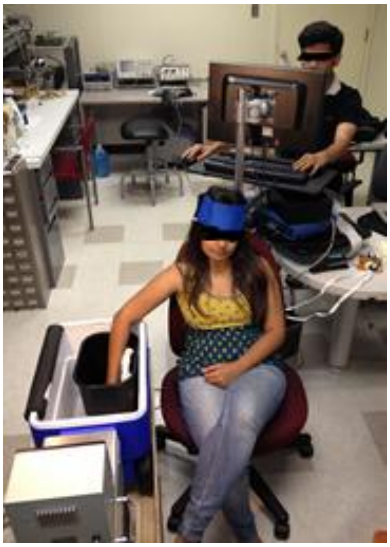

Figure 7: Setup of cold pressor test during the experiment

'Cold pressor tests' at a temperature of 5°C were performed on the subjects for measuring their pain threshold and pain tolerance while recording their fNIR spectroscopy signal in order to compare these parameters with objective measures acquired through fNIR spectroscopy. Before any pain tolerance experiment, subjects were instructed to notify the researcher once he/she starts feeling pain after immersion in cold water and once the pain becomes intolerable for them.

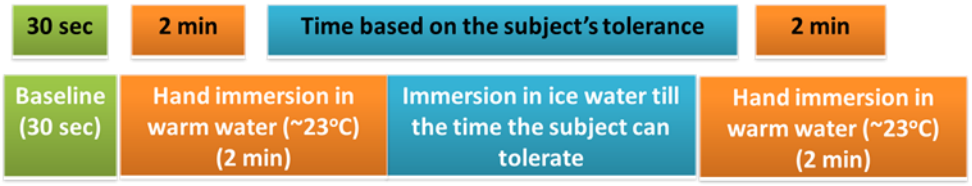

Figure 8: Experimental protocol of pain threshold and tolerance test using cold pressor test

Each experiment consisted of a baseline recording at rest followed by the immersion of the right hand up to the wrist into a bucket of circulating tepid water kept at room temperature (~23°C) for 2 minutes for adaptation. This was then followed by right-hand immersion into cold water (0°C-10°C or 32°F-50°F). Subjects were asked to ring the bell when they felt a pain of 3 on a numerical rating scale from 0 to 10 (NRS-11), where '0' indicates no pain and '10' indicates the worst imaginable pain. Upon experiencing an intolerable pain (10 on the NRS-11), subjects withdrew their hand from the cold water and immersed it back into the room temperature water for 2 minutes for the hemodynamic recovery. The constant temperature bath device RM6 LAUDA Brinkmann was used to cool the water. A block diagram of the protocol is shown in Figure 8. The

pre-stimulus baseline was used as a reference to calculate changes in Hb and HbO2 concentrations. Subjects received an auditory command from the experimenter when to switch their hand from the tepid water into the cold water and vice versa.

3.3 RESULTS

Hemodynamic parameters measured by fNIR spectroscopy (oxy-hemoglobin (HbO_2), deoxy-hemoglobin (Hb), and total hemoglobin (THb)) showed that subjects with high tolerance to pain had HbO_2 and THb curves with signs of adaptation to pain, observed by the gradual curve in the cold-water stimulus consistence with their subjective self-reports. No visible or significant adaptation was observed in those with low tolerance. Hence the results were extremely significant: the more intense pain is felt by the subject, the more the concentration of HbO_2.

A typical fNIR spectroscopy signal resulting from this experiment is shown in Figure 9. The red curve represents oxygenated hemoglobin, the blue curve represents de-oxygenated hemoglobin and the green curve represents the total hemoglobin concentration. The black bars are the markers of the experiment. In the figures given below the first marker indicates the hand-immersion in tepid water, the second marker indicates hand immersion in cold water, the third one indicates the onset of pain i.e. when the subject's self-report of pain becomes 3/10, while the last one indicates the time when the subject took the hand out of cold water and immersed in tepid water i.e. when the subject felt intolerable pain of 10/10 or at the end of 5 minutes immersion in cold water.

It was observed that the subjects could be categorized into two main groups: ones with low tolerance to pain and ones with high tolerance to pain. Adaptation was seen in subjects with high tolerance to pain which could be a result of sensitization of the skin due to cold stimuli. No visible or significant adaptation was observed in subjects with low tolerance to pain as they could not hold the hand long enough to possibly reach a level of sensitization. These observations were found to be consistent with subjective report of pain. A sample self-report for subject with low and high tolerance each is shown in Table 1 and Table 2 and their corresponding levels of oxy and deoxy-hemoglobin concentration as well as total hemoglobin are shown in figure 9 (a and b) and 10 (a and b) for right forehead and left forehead respectively. It was also observed that the signals from near and far channels were similar. The results show that the subject self-report of pain correlated very well with signal. All the data collected from subject of different ages and sex showed similar results.

Time (s)	**0**	**30**
Pain Scale	**3**	**9**

Table 1: Pain Scale (Low Tolerance Subjects)

Time (s)	**0**	**30**	**60**	**90**	**120**	**150**	**180**	**210**	**240**	**270**	**300**
Pain Scale	**3**	**5**	**6**	**7**	**9**	**9**	**8**	**8**	**7**	**7**	**7**

Table 2: Pain Scale (High Tolerance Subjects)

HIGH TOLERANCE

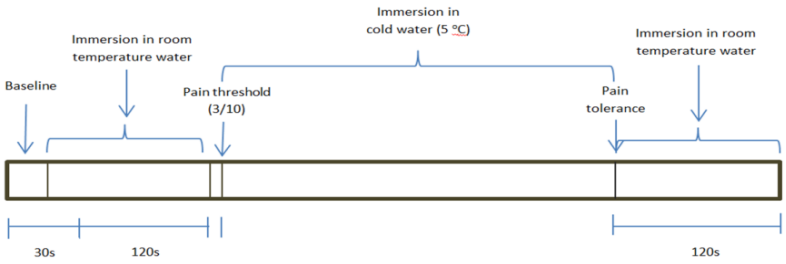

Right Forehead

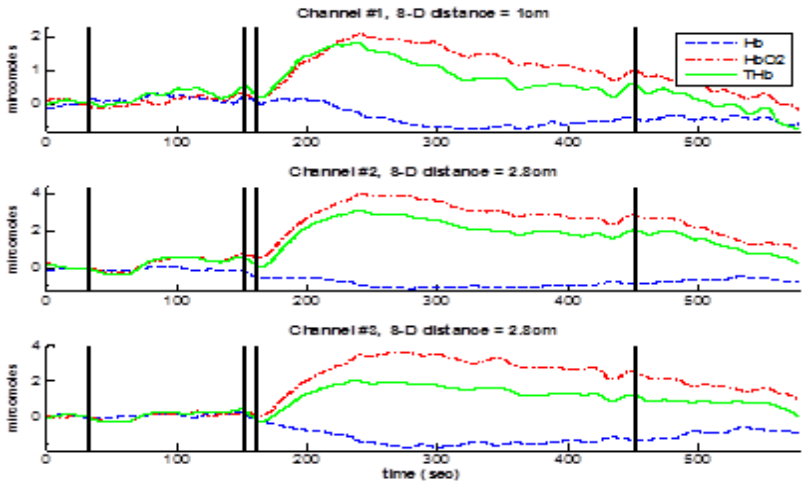

(a)

Left Forehead

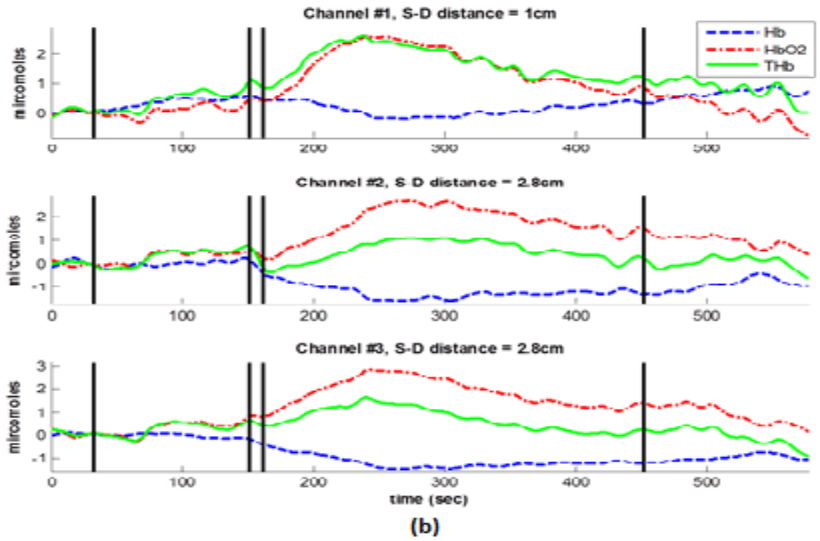

(b)

Figure 9: oxy, de-oxy and total hemoglobin concentration of subject with high tolerance measured at (a) the right forehead and (b) the left forehead

LOW TOLERANCE

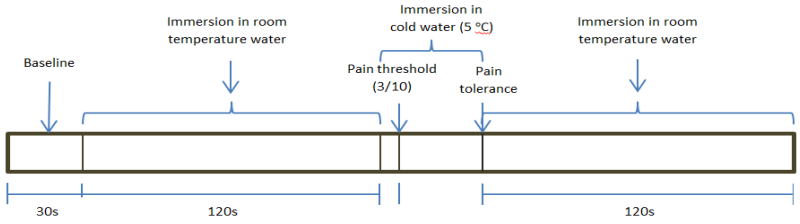

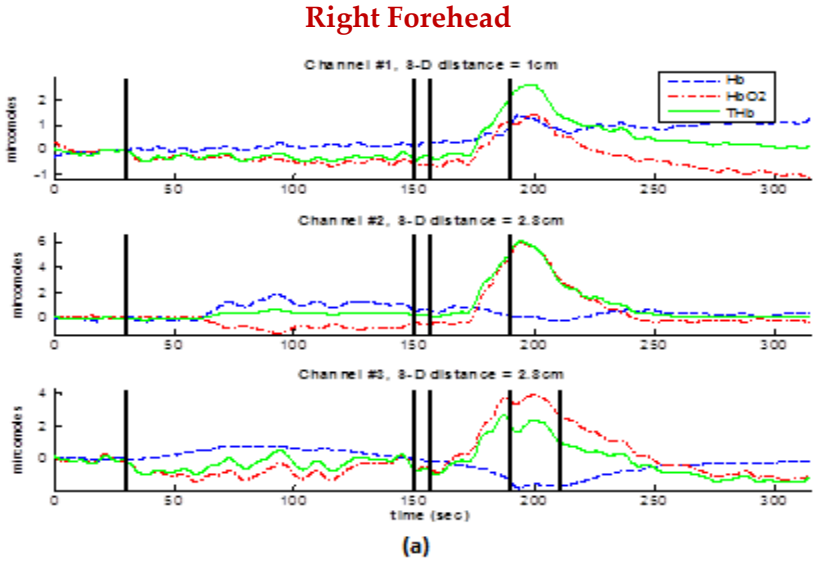

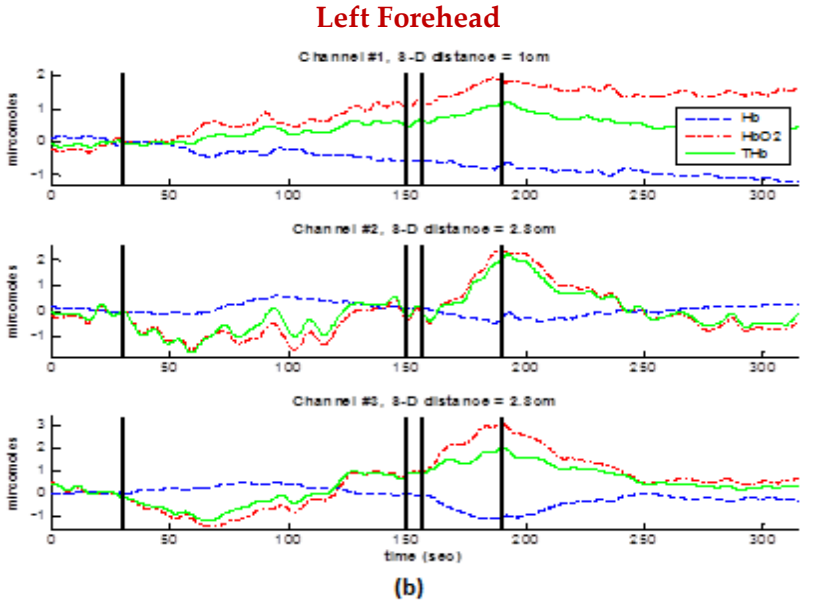

Figure 10: oxy, de-oxy and total hemoglobin concentration of subject with low tolerance measured at (a) the right forehead and (b) the left forehead

The detail analysis of these data sets are not within the scope of this thesis and will be done by our group in future after enough subjects have been tested. However, these experiments showed that the total hemoglobin concentration is markedly different during the presence of cold stimulus as compared to the absence of the stimulus. As the tonic pain induced by noxious cold water is massively confounded and regulated by sympathetic activity, it can be concluded that the observed hemodynamic change in response to the cold water stimulus is mainly dominated by the sympathetic nervous system. However, stimuli that would evoke a less generalized response might provide a different insight to understand the contribution of autonomic nervous system in response to pain. Peltier device has been used for delivery of cold stimuli and it supplies the stimuli to a small surface area of the skin. Thus, this steered us towards using Peltier device for delivering cold noxious stimuli.

CHAPTER 4: PELTIER DEVICE

In order to proceed towards Peltier experiments, the first step was to overhaul an existing Peltier setup. The experimental section of this chapter discusses the homemade Peltier setup along with the steps followed to optimize the appropriate parameters for stimulus delivery, the limitations of the setup, incorporation of a new Peltier device to overcome these limitations and the protocol and procedure followed to run the experiments. The results obtained from the hemodynamic response evoked in the subjects due to cold stimuli from the Peltier device have been presented.

4.1 PRINCIPLE

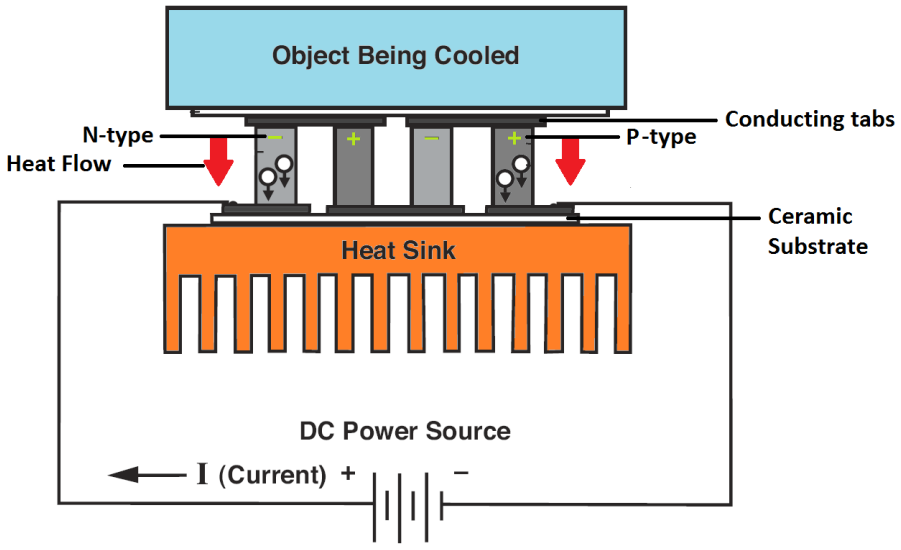

Figure 11: Representation of working principle of Peltier device

A Peltier device consists of alternate p-type and n-type semiconductor nodes connected in series by conducting tabs which are sandwiched between two ceramic substrates.

Each n-type and p-type node-pair forms a thermoelectric couple and the two pairs of n-type and p-type nodes as shown in the Figure 11 is termed a "two-couple module". N-type material is doped so that it will have an excess of electrons and p-type material is doped so that it will have a deficiency of electrons. The extra electrons in the n-type material and the "holes" resulting from the deficiency of electrons in the p-type material are the carriers which move the heat energy through the thermoelectric material. When DC power supply is connected to this series of alternate p-type and n-type nodes, the electrical current starts moving back and forth alternately between the top and bottom substrates through each p-type and n-type node. This series current causes a parallel flow of heat which is perpendicular to the ceramic substrate. Passage of DC current through Peltier device establishes a temperature difference across the two ceramic surfaces of the Peltier device. Once the temperature of one side is pinned down by using a heat sink and a constant temperature bath, then the temperature of the other side can be controlled by varying the direction and the magnitude of the DC current. The temperature difference depends on the magnitude of the input current; the higher the current, the greater the difference. The property of the Peltier device discussed above has been exploited in the following way: When high current of the order of 3 Amperes is applied, one of the ceramic substrates can attain subzero temperature while the other substrate can get excessively heated. The cold substrate can be used for inducing experimental cold stimuli.

4.2 LITERATURE REVIEW

Peltier device has been successfully used for pain studies. Harrison and Davis have studied the psychophysical responses to noxious cold stimulation of the skin in normal human subjects wherein a Peltier stimulator was used to deliver cold stimuli [60]. Defrin et al. have used a Peltier based thermal stimulator to deliver warm and cold stimuli which produces a sensation of pricking pain in human subjects [61]. This was done in order to find out whether the quality of painful thermal sensation (hot or cold) is determined only by conduction in specific nociceptive channels, or is a result of integrated activity in both nociceptive and non-nociceptive channels. Also, Becerra et al. have carried out Functional MRI studies of pain where they have shown that a distinct Digital Optical Tomography signal over the somatosensory cortex to a noxious heat stimulus could be distinguished from the signal elicited by innocuous mechanical stimuli. They had used a Peltier thermode to produce the heat stimuli [62]. Moreover, a psychophysical study by Christopher deCharms et al. about control over brain activation and pain learned by using real-time functional MRI was done by using a Peltier thermode on the subjects' palm to deliver thermal stimuli [63]. An advantage of using Peltier device would be that both cold as well as hot stimuli tests can be performed in the same setup without alteration or delay in experimental factors. In addition to the prevalent use of Peltier device, it has been widely used as part of standard routine at many pain clinics including Hahnemann Hospital, Drexel University. This methodology of delivering stimulus is clinically more convenient as it

reduces subject discomfort in clinical setup and also provides more control to the subject.

4.3 EXPERIMENAL SET UP

The Peltier device explained below was originally developed at Drexel University by Bruno Pecchiura. This device constitutes of one thermo-electric Peltier device, which is controlled by a computer. It requires electronic circuits to control it, and an efficient cooling system to keep it cold. General schematic of the device is presented in Figure 12.

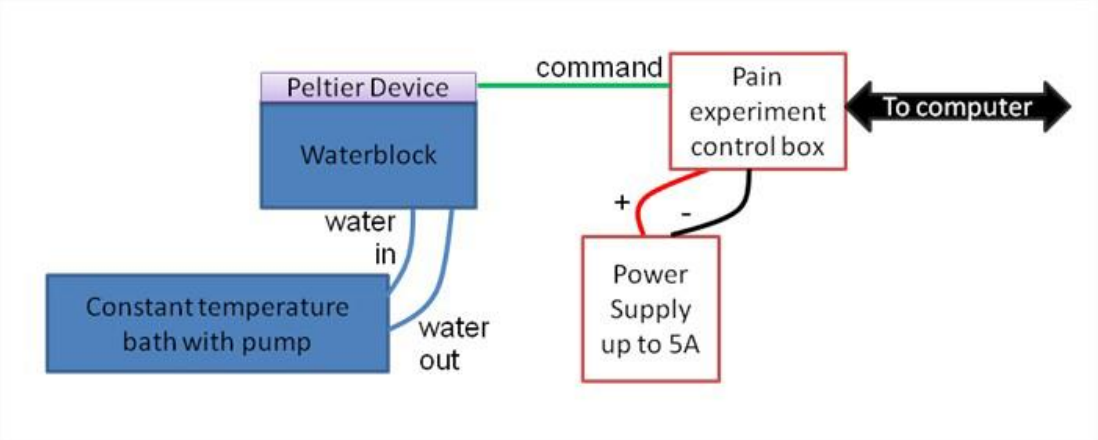

Figure 12: General Schematic of the Peltier setup

This setup constitutes of a Peltier device, which works on the principle mentioned previously. This device dissipates heat to one side and so to avoid the device getting very hot, we need to cool it efficiently. In order to do this, a water-cooled heatsink, also known as a waterblock was used. To have a stable temperature, the water injected in the waterblock was furnished by a constant temperature bath (RM6 LAUDA Brinkmann,

with cooler, heater and pump). The constant temperature bath enabled precise control of the water temperature and allowed for a simpler way to have different pain levels.

Temperature results show that if the current through the device is higher than 2.5 amps, the temperature is rising. This is due to the fact that the Peltier device dissipates a lot of heat and the water-cooling system cannot dissipate it fast enough when there is too much current. Therefore, the device has to be controlled on a range between 1A and 2.5A.

To make the experimental process easier, the device had to be controlled through the computer. In order to do that, an electronic control circuit with a Darlington pair (Figure 13) was created to control the current provided to the Peltier device using specifically made software. The communication to the computer was made by a FTDI FT232R chip, which created a serial interface using a USB port. The output was used to control a DAC (Digital to Analog Converter) using SPI protocol. By using this analog 0 to 5V voltage on the gate of the power Darlington, the current going through the device was limited. It is only controllable on a range between 1 and 2.5 A.

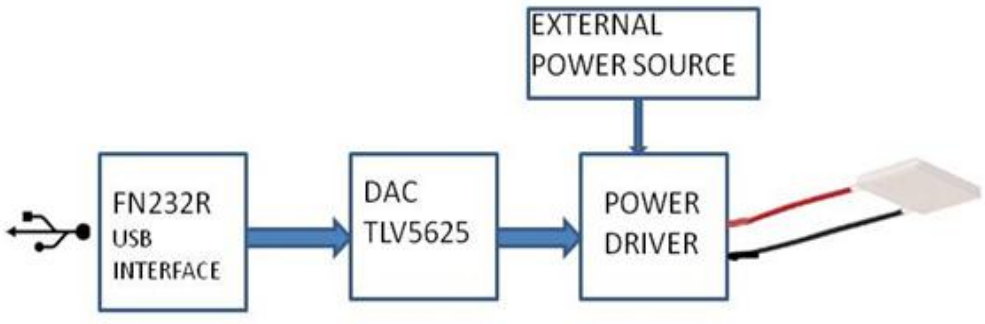

(a)

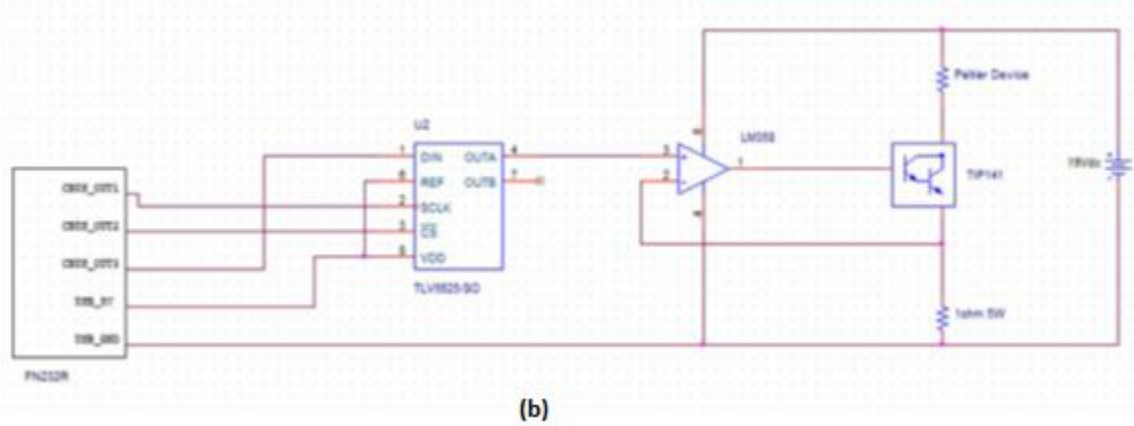

Figure 13: (a) Block diagram representation of control circuit (b) Electronic schematic of control circuit

A program named Automatic Markers For Cobi (AMFC) served as the user interface for controlling the communication of the Peltier device with the computer as well as the amount of current delivered to the device. As shown in the figure below, the communication can be made by marking one or more of the boxes while multiple timings can be mentioned in the boxes shown to the left. The communication will be activated during the time duration where the box is marked, when the Peltier surface would get hot or cold as per the connection. The rate of this change in temperature can be controlled through the six steps of the stimulus intensity option provided in the software where the first corresponds to the least intensity and the last one to the maximum intensity.

4.3.1 OPTIMIZATION OF PARAMETERS

A controlled surface of the Peltier device is critical for experimentation as it is the part of the system exposed to the human subject. According to the system setup, there were two

important factors to be controlled: the minimum and maximum temperature of the exposed surface of the Peltier and the rate of change of the thermal stimulus. Absence of current to the Peltier device would serve as the baseline (adaptation) temperature and this would be maintained through the constant temperature water bath connected to Peltier via the tubing. When the Peltier device communicates with the computer (for marked duration on AMFC), current is supplied to the Peltier device depending on the intensity selected. This determines the rate of change of temperature of the Peltier surface.

A balance of these two parameters would determine the feasibility of the device for use in human experimentation. In order to optimize the timing of the cold and hot stimuli as well as the temperature of the exposed Peltier surface, various trials were carried out. The temperature of water bath was varied in a range of 20-35 ^{o}C and the temperature of the Peltier surface was found to be consistent with an error of about 1 ^{o}C. In order to have a baseline (adaptation) temperature worth inducing a thermally neutral sensation in human skin, a trial window of 25-30 ^{o}C was defined to be the baseline (adaptation) temperature. Following the superposition principle, the stimulus intensity was now varied from intensity of step 1 to step 6 to find an optimum rate of change of temperature and to maintain the Peltier surface at the desired temperature for delivering hot as well as cold stimuli. The amount of current flowing through the Peltier device was measured for each of the stimulus intensities provided by the software and the average readings are shown in Table 3.

Stimulus Intensity	1	2	3	4	5	6
Current (A)	0.8	1.198	1.594	2.02	2.55	2.54

Table 3: Average current through Peltier device for each stimulus intensity provided by AMFC

It was observed that for the Peltier device, a stimulus intensity of 5 on AMFC was optimum to achieve the desired rate of change of temperature for generation of cold stimuli at about 0°C while a stimulus intensity of 1 was enough to achieve desired ramping for generation of hot stimuli of about 49°C. Multiple trials were conducted to generate cold stimuli by keeping baseline temperature (temperature of the constant temperature water bath) and amount of current delivered to the Peltier constant. Figure 14a represents a sample plot of rate of temperature change of the Peltier surface, averaged over six trials, with baseline (adaptation) temperature of about 30°C.

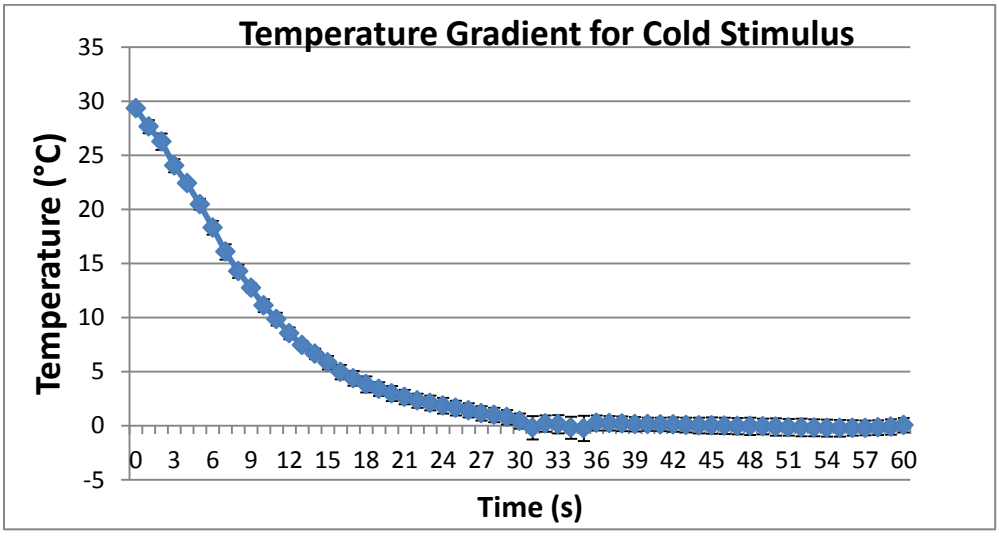

(a)

It was found that it took about 30 seconds for the Peltier to reach the desired temperature of about 0 °C which is cooling rate of about 1 °C/s. Several equivalent trials were conducted to generate heat stimuli. Figure 14b represents a similar plot for heat stimuli, with baseline (adaptation) temperature of about 30°C. It was found that it took about 25 seconds for the Peltier to reach the desired temperature of about 50 °C which is heating rate of about 0.8 °C/s.

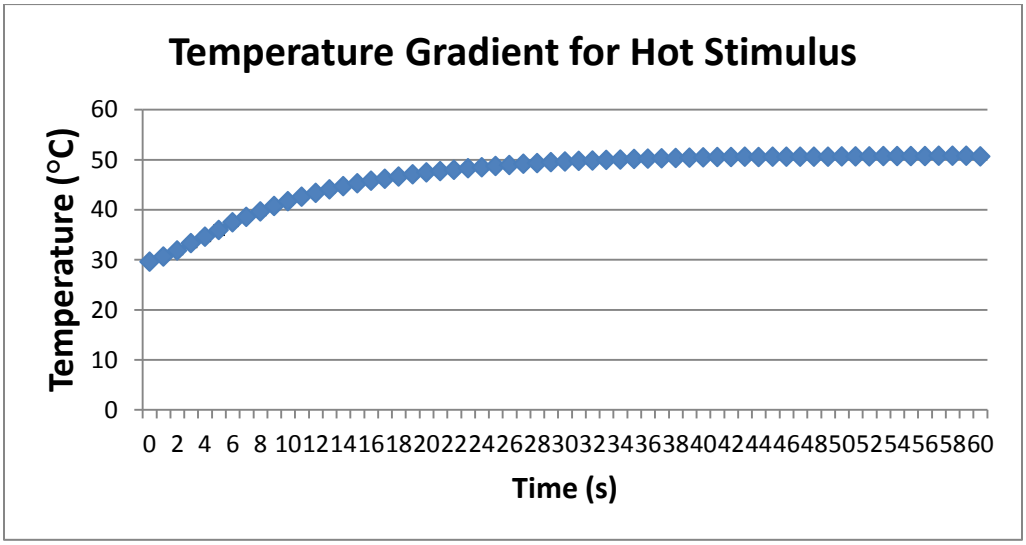

(b)

Figure 14: Plot of averaged readings for rate of temperature change of Peltier surface for delivery of (a) cold stimuli; (b) hot stimuli

4.3.2 LIMITATIONS IN THE SETUP

Although optimization of parameters of the Peltier device paved a way for conducting trials on human skin surface, it was less feasible to conduct actual experiments as the setup, as a whole, posed certain limitations. According to the specifications of the Peltier device it draws up to 6A current while the temperature difference between the two

surfaces that it can handle is ±65°C. The risks from the high current could be avoided by covering it with an insulated surface and avoiding the exposure. However, as mentioned above, the current through the Peltier could be controlled only in 6 steps and thus the baseline temperature had to be set in such a way that it is feasible for thermally neutral sensation for human skin. Also, the current supplied to the Peltier should not allow the temperature difference between its two surfaces to exceed 65 °C. As shown in figure 14 the time it takes to reach the desired temperature from the baseline (adaptation) temperature is about 30 seconds. This means that the current through the Peltier device should be such that the rate of change of temperature should not go beyond 2 °C/s in order to hold the temperature at the desired value. Another limitation of the homemade

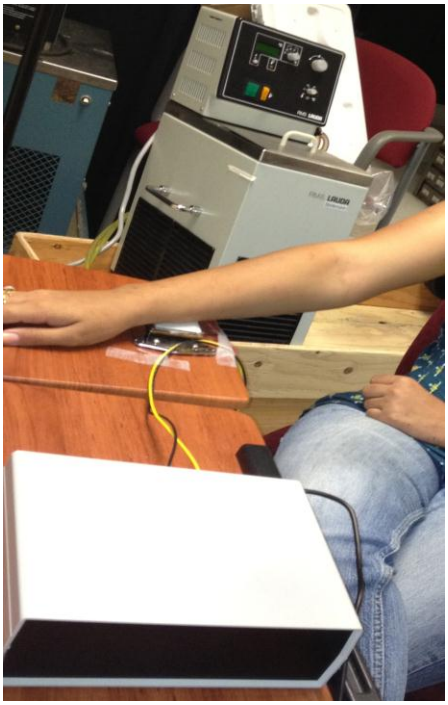

Figure 15: Setup of Peltier device with subject's hand placed on Peltier surface

Peltier setup was that the current supplied to the Peltier device could be controlled in fixed amount of steps. Six stimulus intensities being provided by the AMFC software, the current can be delivered only in fixed amounts corresponding to these six intensities as mentioned in section 4.3.1. In order to gain more control over the temperature of the Peltier surface, more amounts of current delivery would be required. The above mentioned factors like restricted temperature difference between two surfaces of Peltier, limitations of setting the baseline (adaptation) temperature and fixed current intensities, resulted in providing less room to the experimenter to control the parameters for better experimentation. Also, the experiment has to make sure that the temperature of the Peltier surface or the duration of the stimuli or a combination of both stays in the safety limit for human subjects. In addition to this, as per the current setup, if the subjects feel any discomfort they can let the experimenter know who will be able stop the stimulus immediately and return the temperature of the Peltier surface to baseline (adaptation) temperature. The subject himself/herself has very little control over the device which can be considered as one of its limitations. Consequently, the limitations gave rise to need of an alternative device.

4.3.3 INCORPORATION OF NEW DEVICE

Optimization of parameters provided an in-depth knowledge of the principle as well as functioning of Peltier device. However, the limitations prevented a strong, reliable and consistent hemodynamic response as well as data collection. This led to an incorporation of a new FDA approved and commercially available device TSA-II Neuroanalyser

manufactured by Medoc Inc. A working knowledge of the Peltier setup led to efficient use of the new device.

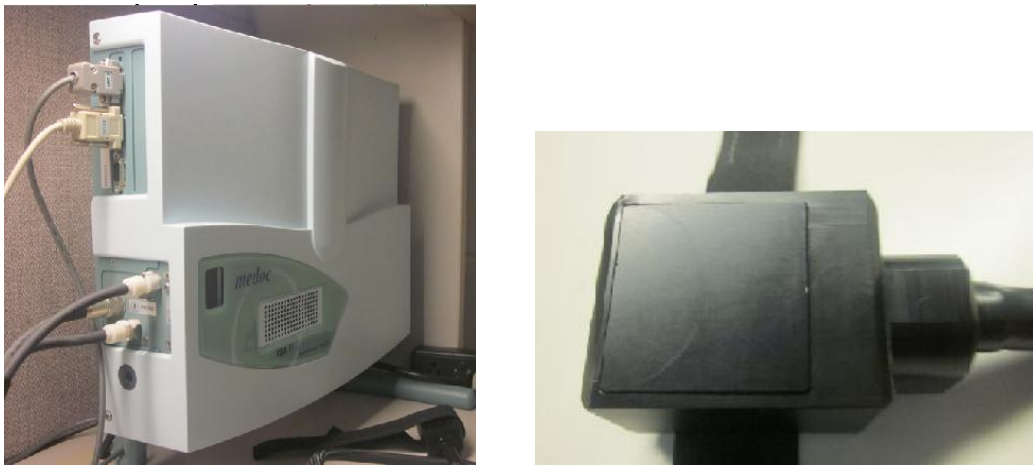

Figure 16: (a) Medoc TSA-II Neuroanalyser (b) Peltier thermode

The system for this Peltier device could be considered similar but more sophisticated as compared to the home-made setup discussed earlier. It consists of a device (Figure 16a) with an inbuilt constant temperature waterbath to maintain the temperature of the Peltier surface, a Peltier thermode (Figure 16b) that can be placed on the subject and a software to control the functioning of the device and the parameters for the experiment including the type of stimuli, type of test, duration of the stimuli, etcetera. This device being computerized, the thermode could be controlled through its communication with a computer where its software is installed. Some of the limitations of the actual setup could be overcome through this device. The Peltier thermode contains 2 temperature sensors and its surface in contact with skin is aluminum coated thus making temperature measurement more accurate. Moreover, the current supplied to the

thermode could be varied at greater precision thus allowing a more controlled and wide range of rate of temperature change. This consequently allows more flexibility in setting the parameters like the baseline (adaptation) temperature, the rate of temperature change, the inter-stimulus interval, the destination temperature and the number of stimuli to be delivered. The safety of humans is accounted for in the Medoc Peltier device as it stops and returns the temperature of the thermode to adaptation temperature in cases when the temperature of the thermode or the duration of stimulus or a combination of both goes beyond the safety limit for humans.

The device has inbuilt functions to carry out various tests by delivering hold or cold stimuli. For example, it can measure sensory thresholds such as the sensation of warmth, cold, heat-induced pain and cold induced pain as well as suprathresholds to allow for quantitative assessment of pain. Thus it provides for a more comprehensive test. One of the methods for this is the method of limits where the stimuli increase in intensity and the subject hits the stop button to stop the stimuli to determine the threshold of thermal sensation or the threshold of thermal pain. Other constant stimuli methods, where stimuli of predetermined intensity are delivered, include method of levels, staircase method and suprathreshold method. The suprathreshold method has been incorporated in our experiments for the delivery of cold painful stimuli. In this method, the subject is exposed to a sequence of stimuli whose intensity surpasses the pain threshold of an individual and the data is then used to extract stimuli-response relationship. Thus,

before appropriate modifications will be made to the home-made Peltier setup, Medoc Peltier device can be used for the delivery of a similar sequence of cold painful stimuli.

4.3.4 PROTOCOL AND PROCEDURE

For providing the cold stimuli for inducing experimental cold pain, a Peltier device, which works on the principle mentioned above, was used.

A pilot study was conducted, wherein ten right-handed healthy individuals (5 males and 5 females) were recruited from amongst the members of Conquer Collaborative Lab with no history of psychological or neurological disorder or any ongoing medication. All the participants were verbally informed about the details of the experiment including the experimental procedure, the kind of stimulus that will be applied to them, the duration of the experiment as well as the main objective of the study and verbal consent was obtained from them before the experiment. They were seated comfortably during the experiment facing away from the experimenter to avoid any distractions.

Two similarly configured fNIRS probes as mentioned previously were secured comfortably on the left and right forehead of the subject using a Velcro strap. The thermode of the Peltier device was attached firmly to the volar surface of the right forearm of the subjects which would supply the cold stimuli to a patch of subjects' skin in contact with the thermode surface (Figure 17). In addition to this, a temperature sensor was attached to the skin along with the thermode, to get an idea of actual skin temperature during the experiment. The power to the LEDs and photodetectors was

supplied through a connector circuit. Raw data from the subjects' forehead was collected at a sampling frequency of 2 Hz.

Figure 17: Peltier thermode attached to the subject's hand

After setting up the system, the software of the device was used to control the stimuli. The option 'Perform a test' was selected from the main screen and the subject details were added through the option of adding patients. Then after, the test method 'Suprathreshold' was selected from the available options, which was followed by selection of 'right forearm medial' as the body site where the thermode was to be placed. This was then followed by attaching the thermode to the subject's forearm and then running the test.

The experiment began with a 120-second rest state at a baseline (adaptation) surface temperature of 27 ^{o}C followed by a decrease block of 7-15s (depending on individual skin and body temperature) where the temperature of the thermode surface reduced upto 32 ^{o}F (0 ^{o}C). The thermode was held at this temperature of 32^{o}F (0 ^{o}C) for 30 seconds. This was then followed by an increase block wherein the temperature of the

thermode increased back to baseline (adaptation) temperature. This was followed by a wait time of 15 seconds. Markers were placed each time when the stimulus returned to 27 °C. Thus the trial window of [15s wait time (baseline temperature of 27 °C) - ~7-15s fall time (temperature falls to 0 °C) - 30s stimulus (at 0 °C) - ~10s rise to baseline (increase to 27 °C)] was repeated 8 times. A post-stimulus baseline of 120s was recorded similar to the initial pre-stimulus baseline. This whole segment of 8 stimuli was repeated 3 times resulting in total of 24 stimuli (Figure 18).

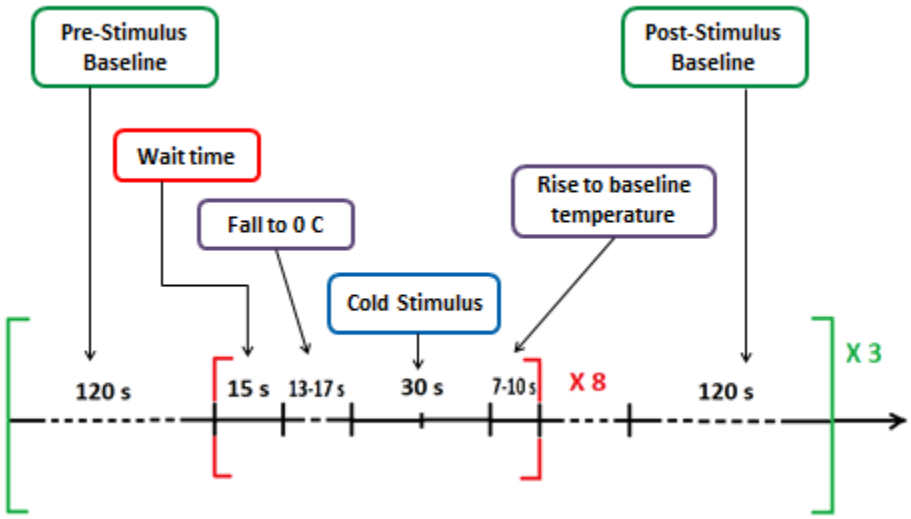

Figure 18: Block diagram of protocol for Peltier experiments

Subjects were verbally asked by the experimenter to rate their pain on a numerical rating scale of 0-10 (NRS-11), where '0' indicates no pain and '10' indicates the worst imaginable pain. Throughout the experiment the room was dimly lit in order to avoid the effect of background light on the data being collected. The ambient temperature was maintained at ~23°C.

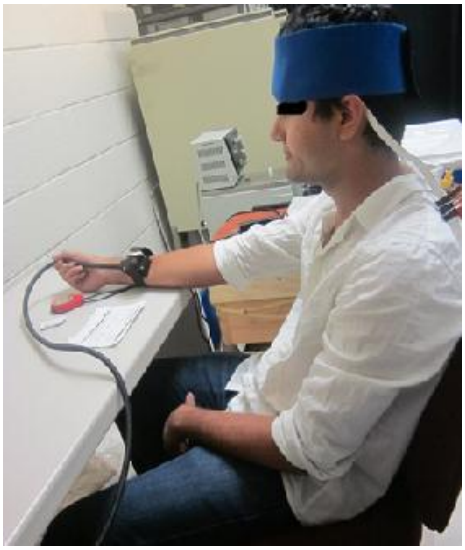

Figure 19: Setup of a Peltier experiment

The decision of selecting specific values for various parameters was aimed towards collecting valuable data while taking subject into consideration. A pre and post stimulus baseline of 2 minutes allowed better feature extraction while the wait time of 15 seconds gave enough time to the skin for adaptation and in getting back to baseline (adaptation) temperature. Duration of 30 seconds was chosen for delivery of the cold stimulus to generate enough hemodynamic response and avoid sensitization of the subjects' skin. As the SNR (Signal to Noise Ratio) in fNIR studies is very low, the stimulus was delivered 24 times in order to obtain a reliable data by averaging the signals from all trials. Dividing these 24 trials of stimulus delivery into 3 parts with 8 stimuli in each part, was aimed at avoiding subject boredom while simultaneously adding reliability to the results.

4.4 RESULTS

Hemodynamic parameters measured by fNIR spectroscopy in response to cold stimuli through Peltier device showed that a detectable response can be generated through repeated cold stimuli over a small surface of skin. The plots shown below represent an average response of oxy and deoxy-hemoglobin from right and left forehead averaged from a total of 24 stimuli. The average pain rating as reported by subjects from these trials was 4.8 on the NRS-11 scale. In the plots, the first marker represents the start of a stimulus. The second marker shows the time at which the temperature of the probe reaches 0°C and the third marker shows the time at which the temperature of the Peltier thermode starts to return to the baseline (adaptation) temperature.

Averaged Response for 10 Subjects (Averaged Pain Rating = 4.8)

Right Forehead

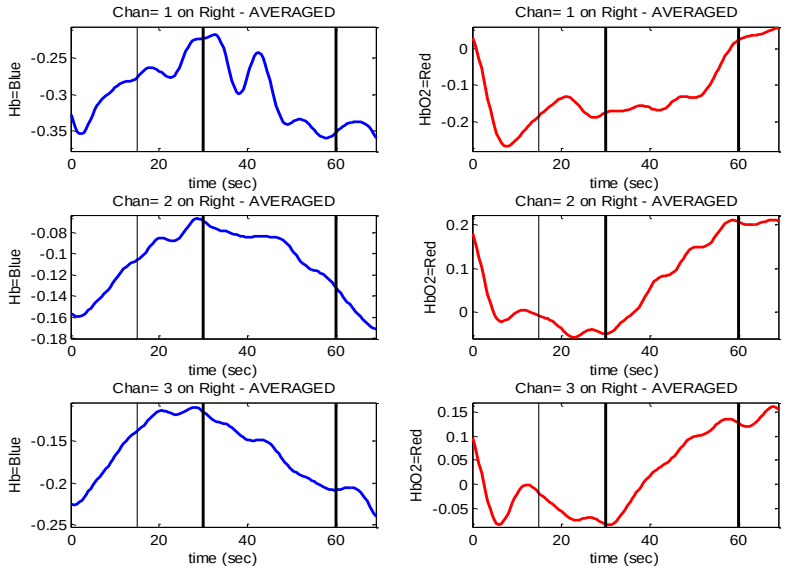

(a)

Left Forehead

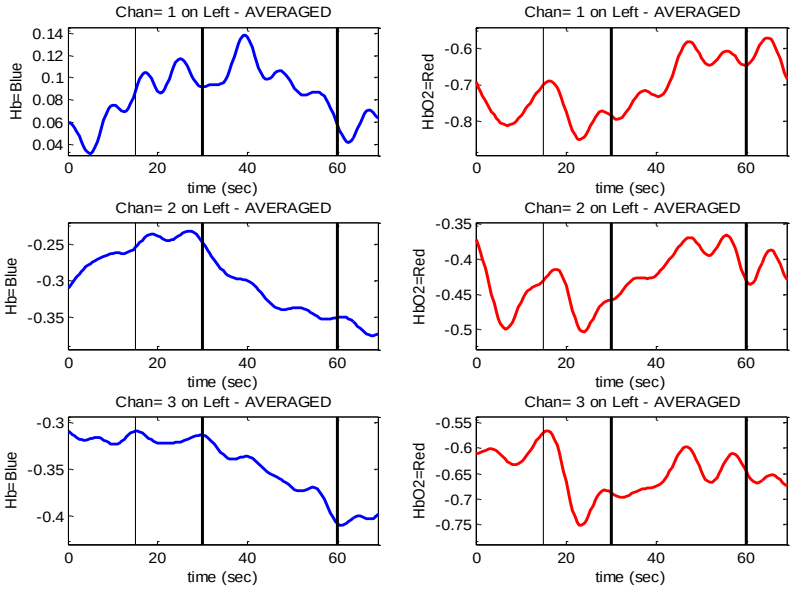

(b)

Figure 20: Averaged Response of oxy and deoxy hemoglobin concentration for 10 subjects from (a) Right forehead and (b) left forehead; Peltier stimulus

A drop in the deoxy hemoglobin concentration is seen during the presence of cold stimuli while a clear rise in the oxy-hemoglobin concentration is seen during the same period. It can be seen from the plots that after the second marker i.e. when the temperature of the Peltier thermode has reached 0^{o}C a noticeable change in concentrations of oxy and deoxy-hemoglobin is measured.

These results indicate that successful experiments could be carried out and biologically useful data could thus be extracted by using Peltier device. This was made possible by the comprehensive knowledge of the working of Peltier device gained in the process of hardware improvement of the homemade Peltier, optimization of parameters and the

protocol as well as hardware development for the fNIR spectroscopy system. However, the detail analysis of these data sets are not within the scope of this thesis and will be done by our group in future after enough subjects have been tested. With further modifications and refinement in the homemade Peltier setup, it has a potential use in pain research with fNIR spectroscopy. The conclusions from the study as well as some suggestions for future research have been discussed in the next section.

CHAPTER 5: CONCLUSIONS

In summary, the experimental setup, protocol as well as the procedure was efficaciously prepared such that successful clinical trials can take place and the results of the pilot studies indicate that the goals mentioned initially have been achieved. The present research work aimed at developing the hardware, overcoming the flaws in the system set up as well as to optimize various parameters for experiments so as to improve the quality of experimentation. This included troubles in signal acquisition using the home-made fNIR sensors from the near channels, development of an adapter circuit for operation of the correct channels from the control circuit used to operate the infrared light source and photodetectors, optimization of parameters of the home made Peltier device for safe human experimentation as well as optimizing the protocol for acquiring detectable hemodynamic response from Medoc Peltier device. Successful pilot tests to measure hemodynamic response using fNIR spectroscopy were carried out using cold pressor tests as well as cold stimuli through Peltier device and hemodynamic changes could be seen during both types of cold painful stimuli. It was seen that in the cold pressor tests, the fNIR spectroscopy results of the hemodynamic response correlated well with the subjective reports of pain. A similarity between the signals from the far and near channels of the fNIR sensors was also observed. As a result of trial and error method of changing the baseline (adaptation) temperature and the amount of current supplied to the Peltier element, an optimum range of parameters were efficaciously defined and with some refinements, it can be used for conducting experiments.

Moreover, taking various factors like better feature extraction, data reliability as well as comfort and interest of subject, into consideration, an optimum protocol for Peltier experiments using Medoc Peltier was developed. The fNIR spectroscopy results of hemodynamic response using Peltier device for delivery of cold stimuli showed a possibility of less generalized hemodynamic response. These results show that fNIR spectroscopy is a promising technology for monitoring hemodynamic response to acute pain at different depths and is also a potential technology to investigate the underlying mechanisms leading to cold allodynia in chronic pain patients.

5.1 SUGGESTIONS FOR FUTURE

In order to take a step forward towards exploring the further use of fNIR technology to understand the hemodynamic response to pain, certain refinements would be needed in the current experimentation. The current fNIR sensor design has been a tradeoff between flexibility and light weight versus higher number of channels for more accurate data. A newer probe configuration with more channels with multiple source-detector distances would allow a more precise hemodynamic response along with data acquisition from multiple sites in the brain and skin. The current subject pool size could be considered reasonable to show the usability of the hardware development; however, to improve the reliability of the results and to gain more in-depth knowledge of the hemodynamic response, collection of data from a larger sample size is necessary. In addition to this, to assess the contribution of the cortex and superficial tissues in the measured signal, advanced signal processing techniques are essential.

As the experiments with delivery of cold stimuli through the Peltier device are in the developing stage at our lab, it gives rise to the need of some further modifications in the experimentation. In order to use the existing homemade Peltier setup for conducting experiments, more refinements should be made with the goal of increasing control over the stimuli and subject safety and comfort. Advanced hardware which would allow more control over the flow of current in the Peltier device would provide more control over the delivery of cold stimulus for the experimenter. A temperature sensor could be embedded in the surface of the Peltier in contact with the subject's skin to improve the accuracy of the measured temperature. An alarm system which would stop the Peltier device in case of the Peltier surface temperature or the duration of stimulus or both, crossing the safety limit for human subjects, would aid in better experimentation. Also, a press button, which can be pressed by the subject if they feel any discomfort, can be added in the system to provide more control to the subject.

The Peltier experiments done so far were beneficial in understanding the presence of hemodynamic response to repeated cold stimuli. Further exploration can be conducted by incorporating painful heat stimuli in addition to the painful cold stimuli as well as by comparing the responses obtained from the delivery of both kinds of thermal noxious stimuli. Furthermore, conducting similar experiments in patients suffering from cold allodynia might prove useful in understanding the mechanism that lead to the condition in chronic pain patients by comparing the hemodynamic changes in these patients with those in normal subjects.

LIST OF REFERENCES

[1] W. H. Cordell, K. K. Keene, B. K. Giles, J. B. Jones, J. H. Jones, and E. J. Brizendine, "The high prevalence of pain in emergency medical care," *American Journal of Emergency Medicine,* vol. 20, pp. 165-169, May 2002.

[2] J. D. Loeser and R. Melzack, "Pain: an overview," *Lancet,* vol. 353, pp. 1607-1609, May 1999.

[3] "Global Industry Analysts, Inc. Report, January 10, 2011. http://www.prweb.com/pdfdownload/8052240.pdf."

[4] *The American Academy of Pain Medicine*. Available: http://www.painmed.org/patientcenter/facts_on_pain.aspx

[5] D. A. Boas, T. Gaudette, G. Strangman, X. F. Cheng, J. J. A. Marota, and J. B. Mandeville, "The accuracy of near infrared spectroscopy and imaging during focal changes in cerebral hemodynamics," *NeuroImage,* vol. 13, pp. 76-90, Jan 2001.

[6] R. Peyron, L. Garcia-Larrea, M. C. Gregoire, N. Costes, P. Convers, F. Lavenne, F. Mauguiere, D. Michel, and B. Laurent, "Haemodynamic brain responses to acute pain in humans - Sensory and attentional networks," *Brain,* vol. 122, pp. 1765-1779, Sep 1999.

[7] M. G. Sowa, L. Leonardi, J. R. Payette, J. S. Fish, and H. H. Mantsch, "Near infrared spectroscopic assessment of hemodynamic changes in the early post-burn period," *Burns,* vol. 27, pp. 241-249, May 2001.

[8] A. Villringer, J. Planck, C. Hock, L. Schleinkofer, and U. Dirnagl, "Near infrared spectroscopy (NIRS): A new tool to study hemodynamic changes during activation of brain function in human adults," *Neuroscience Letters,* vol. 154, pp. 101-104, 1993.

[9] K. L. Casey, S. Minoshima, K. L. Berger, R. A. Koeppe, T. J. Morrow, and K. A. Frey, "POSITRON EMISSION TOMOGRAPHIC ANALYSIS OF CEREBRAL STRUCTURES ACTIVATED SPECIFICALLY BY REPETITIVE NOXIOUS HEAT STIMULI," *Journal of Neurophysiology,* vol. 71, pp. 802-807, Feb 1994.

[10] K. L. Casey, S. Minoshima, T. J. Morrow, and R. A. Koeppe, "Comparison of human cerebral activation patterns during cutaneous warmth, heat pain, and deep cold pain," *Journal of Neurophysiology,* vol. 76, pp. 571-581, Jul 1996.

[11] R. C. Coghill, J. D. Talbot, A. C. Evans, E. Meyer, A. Gjedde, M. C. Bushnell, and G. H. Duncan, "DISTRIBUTED-PROCESSING OF PAIN AND VIBRATION BY THE HUMAN BRAIN," *Journal of Neuroscience,* vol. 14, pp. 4095-4108, Jul 1994.

[12] A. D. Craig, E. M. Reiman, A. Evans, and M. C. Bushnell, "Functional imaging of an illusion of pain," *Nature,* vol. 384, pp. 258-260, Nov 21 1996.

[13] S. Duschek, N. Hellmann, K. Merzoug, G. A. Reyes del Paso, and N. S. Werner, "Cerebral Blood Flow Dynamics During Pain Processing Investigated by Functional Transcranial Doppler Sonography," *Pain Medicine,* vol. 13, pp. 419-426, Mar 2012.

[14] M. J. Iadarola, K. F. Berman, T. A. Zeffiro, M. G. Byas-Smith, R. H. Gracely, M. B. Max, and G. J. Bennett, "Neural activation during acute capsaicin-evoked pain and allodynia assessed with PET," *Brain,* vol. 121, pp. 931-947, May 1998.

[15] J. Lorenz, S. Minoshima, and K. L. Casey, "Keeping pain out of mind: the role of the dorsolateral prefrontal cortex in pain modulation," *Brain,* vol. 126, pp. 1079-1091, May 2003.

[16] P. Rainville, G. H. Duncan, D. D. Price, B. Carrier, and M. C. Bushnell, "Pain affect encoded in human anterior cingulate but not somatosensory cortex," *Science,* vol. 277, pp. 968-971, Aug 1997.

[17] R. Slater, A. Cantarella, S. Gallella, A. Worley, S. Boyd, J. Meek, and M. Fitzgerald, "Cortical pain responses in human infants," *Journal of Neuroscience,* vol. 26, pp. 3662-3666, Apr 2006.

[18] J. D. Talbot, S. Marrett, A. C. Evans, E. Meyer, M. C. Bushnell, and G. H. Duncan, "MULTIPLE REPRESENTATIONS OF PAIN IN HUMAN CEREBRAL-CORTEX," *Science,* vol. 251, pp. 1355-1358, Mar 1991.

[19] M. Izzetoglu, K. Izzetoglu, S. Bunce, H. Ayaz, A. Devaraj, B. Onaral, and K. Pourrezaei, "Functional near-infrared neuroimaging," *Neural Systems and Rehabilitation Engineering, IEEE Transactions on,* vol. 13, pp. 153-159, 2005.

[20] K. Pourrezaei, Z. Barati, P. Shewokis, M. Izzetoglu, R. Polikar, and G. Mychaskiw, "Hemodynamic response to repeated noxious cold pressor tests measured by functional near infrared spectroscopy on forehead," *Annals of Biomedical Engineering,* 2012.

[21] A. Bozkurt, A. Rosen, H. Rosen, and B. Onaral, "A portable near infrared spectroscopy system for bedside monitoring of newborn brain," *BioMedical Engineering OnLine,* vol. 4, pp. 29-29, 2005 Apr 2005.

[22] H. Rosen, M. Izzetoglu, A. Rosen, B. Onaral, M. Hiatt, M. Anwar, and A. Bozkurt, "The Effect of Auditory Stimulation upon Cerebral Blood Oxygenation in Infants: Measurements by Light Emitting Diode (LED) Near Infrared Spectroscopy," *Conference proceedings : ... Annual International Conference of the IEEE Engineering in Medicine and Biology Society. IEEE Engineering in Medicine and Biology Society. Conference,* vol. 2, pp. 1457-60, 2005 2005.

[23] C.-W. Sun and C.-C. Chuang, "Hemodynamics Study Based on Near-Infrared Optical Assessment, Hemodynamics - New Diagnostic and Therapeutic Approaches," 2012.

[24] Y. Hoshi, "Functional near-infrared spectroscopy: current status and future prospects," *J Biomed Opt,* vol. 12, p. 062106, Nov-Dec 2007.

[25] A. Bozkurt and B. Onaral, "Safety assessment of near infrared light emitting diodes for diffuse optical measurements," *Biomed Eng Online,* vol. 3, p. 9, Mar 22 2004.

[26] B. Chance, E. Anday, S. Nioka, S. Zhou, L. Hong, K. Worden, C. Li, T. Murray, Y. Ovetsky, D. Pidikiti, and R. Thomas, "A novel method for fast imaging of brain function, non-invasively, with light," *Optics Express,* vol. 2, pp. 411-423, 1998.

[27] B. Chance, "Near-infrared images using continuous, phase-modulated, and pulsed light with quantitation of blood and blood oxygenation," *Annals of New York Academy of Sciences,* vol. 838, pp. 29-45, Feb 9 1998.

[28] A. Villringer and B. Chance, "Non-invasive optical spectroscopy and imaging of human brain function," *Trends Neurosci,* vol. 20, pp. 435-42, Oct 1997.

[29] A. Villringer, J. Planck, C. Hock, L. Schleinkofer, and U. Dirnagl, "Near infrared spectroscopy (NIRS): a new tool to study hemodynamic changes during activation of brain function in human adults," *Neurosci Lett,* vol. 154, pp. 101-4, May 14 1993.

[30] B. Chance, Z. Zhuang, C. UnAh, C. Alter, and L. Lipton, "Cognition-activated low-frequency modulation of light absorption in human brain," *Proc Natl Acad Sci U S A,* vol. 90, pp. 3770-4, Apr 15 1993.

[31] B. Chance, "Optical method," *Annual review of biophysics and biophysical chemistry,* vol. 20, pp. 1-30, 1991.

[32] F. F. Jobsis, "Noninvasive, infrared monitoring of cerebral and myocardial oxygen sufficiency and circulatory parameters," *Science,* vol. 198, pp. 1264-7, Dec 23 1977.

[33] H. Obrig and A. Villringer, "Beyond the visible--imaging the human brain with light," *J Cereb Blood Flow Metab,* vol. 23, pp. 1-18, Jan 2003.

[34] H. Obrig, R. Wenzel, M. Kohl, S. Horst, P. Wobst, J. Steinbrink, F. Thomas, and A. Villringer, "Near-infrared spectroscopy: does it function in functional activation studies of the adult brain?," *International Journal of Psychophysiology,* vol. 35, pp. 125-142, 2000.

[35] A. Villringer and B. Chance, "Non-invasive optical spectroscopy and imaging of human brain function," *Trends in Neurosciences,* vol. 20, pp. 435-442, Oct 1997.

[36] F. F. Jöbsis, "Noninvasive, Infrared Monitoring of Cerebral and Myocardial Oxygen Sufficiency and Circulatory Parameters," *Science,* vol. 198, pp. 1264-1267, 1977.

[37] J. S. Soul and A. J. du Plessis, "Near-infrared spectroscopy," *Seminars in Pediatric Neurology,* vol. 6, pp. 101-110, 1999.

[38] H. Ayaz, P. A. Shewokis, S. Bunce, K. Izzetoglu, B. Willems, and B. Onaral, "Optical brain monitoring for operator training and mental workload assessment," *Neuroimage,* vol. 59, pp. 36-47, 2012.

[39] H. Ayaz, M. P. Cakir, K. Izzetoglu, A. Curtin, P. A. Shewokis, S. C. Bunce, and B. Onaral, "Monitoring expertise development during simulated UAV piloting tasks using optical brain imaging," in *Aerospace Conference, 2012 IEEE*, 2012, pp. 1-11.

[40] H. Ayaz, S. Bunce, P. Shewokis, K. Izzetoglu, B. Willems, and B. Onaral, "Using Brain Activity to Predict Task Performance and Operator Efficiency," in *Advances in Brain Inspired Cognitive Systems*. vol. 7366, H. Zhang, A. Hussain, D. Liu, and Z. Wang, Eds., ed: Springer Berlin / Heidelberg, 2012, pp. 147-155.

[41] H. Ayaz, P. A. Shewokis, A. Curtin, M. Izzetoglu, K. Izzetoglu, and B. Onaral, "Using MazeSuite and Functional Near Infrared Spectroscopy to Study Learning in Spatial Navigation," *J Vis Exp,* p. e3443, 2011.

[42] H. Ayaz, P. A. Shewokis, S. Bunce, and B. Onaral, "An optical brain computer interface for environmental control," *IEEE Engineering in Medicine and Biology Society,EMBC,* pp. 6327-6330, 2011.

[43] H. Ayaz, "Functional Near Infrared Spectroscopy based Brain Computer Interface," PhD Thesis, School of Biomedical Engineering Science & Health Systems, Drexel University, Philadelphia, PA, 2010.

[44] H. Ayaz, P. Shewokis, S. Bunce, M. Schultheis, and B. Onaral, "Assessment of Cognitive Neural Correlates for a Functional Near Infrared-Based Brain Computer Interface System," in *Foundations of Augmented Cognition. Neuroergonomics and Operational Neuroscience*, D. Schmorrow, Ed., ed, 2009, pp. 699-708.

[45] H. Ayaz, M. Izzetoglu, S. Bunce, T. Heiman-Patterson, and B. Onaral, "Detecting cognitive activity related hemodynamic signal for brain computer interface using functional near infrared spectroscopy," *Conf Proc 3rd IEEE/EMBS on Neural Eng,* pp. 342-345, 2007.

[46] H. Ayaz, M. Izzetoglu, S. M. Platek, S. Bunce, K. Izzetoglu, K. Pourrezaei, and B. Onaral, "Registering fNIR data to brain surface image using MRI templates," *Conf Proc IEEE Eng Med Biol Soc,* pp. 2671-4, 2006.

[47] M. Izzetoglu, K. Izzetoglu, S. Bunce, H. Ayaz, A. Devaraj, B. Onaral, and K. Pourrezaei, "Functional near-infrared neuroimaging," *IEEE Trans Neural Syst Rehabil Eng,* vol. 13, pp. 153-9, Jun 2005.

[48] K. Sweeney, H. Ayaz, T. Ward, M. Izzetoglu, S. McLoone, and B. Onaral, "A Methodology for Validating Artifact Removal Techniques for Physiological Signals," *Information Technology in Biomedicine, IEEE Transactions on,* vol. PP, pp. 1-1, 2012.

[49] K. Izzetoglu, S. Bunce, B. Onaral, K. Pourrezaei, and B. Chance, "Functional Optical Brain Imaging Using Near-Infrared During Cognitive Tasks," *International Journal of Human-Computer Interaction,* vol. 17, pp. 211-227, 2004.

[50] A. Villringer and U. Dirnagl, *Optical imaging of brain function and metabolism 2* vol. Volume 413. Springer, Jun 30, 1997.

[51] K. C. Kregel, D. R. Seals, and R. Callister, "SYMPATHETIC NERVOUS-SYSTEM ACTIVITY DURING SKIN COOLING IN HUMANS - RELATIONSHIP TO STIMULUS-INTENSITY AND PAIN SENSATION," *Journal of Physiology-London,* vol. 454, pp. 359-371, Aug 1992.

[52] M. D. Papademetriou, I. Tachtsidis, M. Banaji, M. J. Elliott, A. Hoskote, and C. E. Elwell, "Regional cerebral oxygenation measured by multichannel near-infrared spectroscopy (optical topography) in an infant supported on venoarterial extracorporeal membrane oxygenation," *Journal of Thoracic and Cardiovascular Surgery,* vol. 141, pp. E31-E33, May 2011.

[53] T. W. L. Scheeren, P. Schober, and L. A. Schwarte, "Monitoring tissue oxygenation by near infrared spectroscopy (NIRS): background and current applications," *Journal of Clinical Monitoring and Computing,* vol. 26, pp. 279-287, Aug 2012.

[54] E. A. Hines and G. E. Brown, "A standard stimulus for measuring vasomotor reactions: Its application in the study of hypertension.," *Mayo Clin. Proc., ,* pp. 7:332-335,, 1932.

[55] J. M. Stocks, N. A. S. Taylor, M. J. Tipton, and J. E. Greenleaf, "Human physiological responses to cold exposure," *Aviation Space and Environmental Medicine,* vol. 75, pp. 444-457, May 2004.

[56] A. Streff, L. K. Kuehl, G. Michaux, and F. Anton, "Differential physiological effects during tonic painful hand immersion tests using hot and ice water," *European Journal of Pain,* vol. 14, pp. 266-272, Mar 2010.

[57] M. Wolf, M. Ferrari, and V. Quaresima, "Progress of near-infrared spectroscopy and topography for brain and muscle clinical applications," *Journal of Biomedical Optics,* vol. 12, Nov-Dec 2007.

[58] N. E. Walsh, L. Schoenfeld, S. Ramamurthy, and J. Hoffman, "NORMATIVE MODEL FOR COLD PRESSOR TEST," *American Journal of Physical Medicine & Rehabilitation,* vol. 68, pp. 6-11, Feb 1989.

[59] L. A. Mitchell, R. A. R. MacDonald, and E. E. Brodie, "Temperature and the cold pressor test," *Journal of Pain,* vol. 5, pp. 233-237, May 2004.

[60] J. L. K. Harrison and K. D. Davis, "Cold-evoked pain varies with skin type and cooling rate: a psychophysical study in humans," *Pain,* vol. 83, pp. 123-135, Nov 1999.

[61] R. Defrin, A. Ohry, N. Blumen, and G. Urca, "Sensory determinants of thermal pain," *Brain,* vol. 125, pp. 501-510, Mar 2002.

[62] L. Becerra, W. Harris, M. Grant, E. George, D. Boas, and D. Borsook, "Diffuse Optical Tomography Activation in the Somatosensory Cortex: Specific Activation by Painful vs. Non-Painful Thermal Stimuli," *Plos One,* vol. 4, Nov 2009.

[63] R. C. deCharms, F. Maeda, G. H. Glover, D. Ludlow, J. M. Pauly, D. Soneji, J. D. E. Gabrieli, and S. C. Mackey, "Control over brain activation and pain learned by using real-time functional MRI," *Proceedings of the National Academy of Sciences of the United States of America,* vol. 102, pp. 18626-18631, Dec 2005.

APPENDIX A: DATASHEET OF PHOTO-DETECTOR OPT-101

SBBS002A – JANUARY 1994 – REVISED OCTOBER 2003

MONOLITHIC PHOTODIODE AND SINGLE-SUPPLY TRANSIMPEDANCE AMPLIFIER

FEATURES

- **SINGLE SUPPLY: +2.7 to +36V**
- **PHOTODIODE SIZE: 0.090 x 0.090 inch**
- **INTERNAL 1MΩ FEEDBACK RESISTOR**
- **HIGH RESPONSIVITY: 0.45A/W (650nm)**
- **BANDWIDTH: 14kHz at R_F = 1MΩ**
- **LOW QUIESCENT CURRENT: 120μA**
- **AVAILABLE IN 8-PIN DIP AND 8-LEAD SURFACE-MOUNT PACKAGES**

APPLICATIONS

- **MEDICAL INSTRUMENTATION**
- **LABORATORY INSTRUMENTATION**
- **POSITION AND PROXIMITY SENSORS**
- **PHOTOGRAPHIC ANALYZERS**
- **BARCODE SCANNERS**
- **SMOKE DETECTORS**
- **CURRENCY CHANGERS**

DESCRIPTION

The OPT101 is a monolithic photodiode with on-chip transimpedance amplifier. Output voltage increases linearly with light intensity. The amplifier is designed for single or dual power-supply operation, making it ideal for battery-operated equipment.

The integrated combination of photodiode and transimpedance amplifier on a single chip eliminates the problems commonly encountered in discrete designs such as leakage current errors, noise pick-up, and gain peaking due to stray capacitance. The 0.09 x 0.09 inch photodiode is operated in the photoconductive mode for excellent linearity and low dark current.

The OPT101 operates from +2.7V to +36V supplies and quiescent current is only 120μA. It is available in clear plastic 8-pin DIP, and J-formed DIP for surface mounting. Temperature range is 0°C to +70°C.

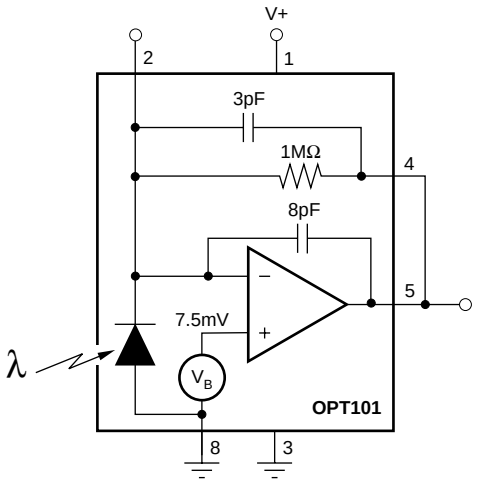

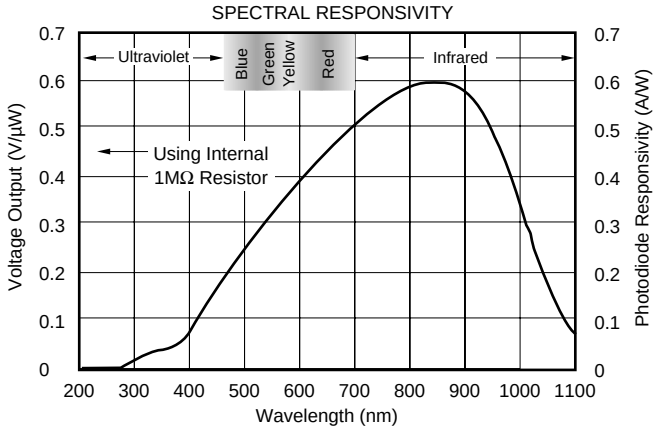

Please be aware that an important notice concerning availability, standard warranty, and use in critical applications of Texas Instruments semiconductor products and disclaimers thereto appears at the end of this data sheet.

All trademarks are the property of their respective owners.

PRODUCTION DATA information is current as of publication date. Products conform to specifications per the terms of Texas Instruments standard warranty. Production processing does not necessarily include testing of all parameters.

Copyright © 1994-2003, Texas Instruments Incorporated

TEXAS INSTRUMENTS
www.ti.com

SPECIFICATIONS

At T_A = +25°C, V_S = +2.7V to +36V, λ = 650nm, internal 1MΩ feedback resistor, and R_L = 10kΩ, unless otherwise noted.

PARAMETER	CONDITIONS	OPT101P MIN	OPT101P TYP	OPT101P MAX	UNITS
RESPONSIVITY					
Photodiode Current	650nm		0.45		A/W
Voltage Output	650nm		0.45		V/µW
vs Temperature			100		ppm/°C
Unit to Unit Variation	650nm		±5		%
Nonlinearity(1)	FS Output = 24V		±0.01		% of FS
Photodiode Area	(0.090 x 0.090in)		0.008		in^2
	(2.29 x 2.29mm)		5.2		mm^2
DARK ERRORS, RTO(2)					
Offset Voltage, Output		+5	+7.5	+10	mV
vs Temperature			±10		µV/°C
vs Power Supply	V_S = +2.7V to +36V		10	100	µV/V
Voltage Noise, Dark, f_B = 0.1Hz to 20kHz	V_S = +15V, V_{PIN3} = –15V		300		µVrms
TRANSIMPEDANCE GAIN					
Resistor			1		MΩ
Tolerance, P			±0.5	±2	%
W			±0.5		%
vs Temperature			±50		ppm/°C
FREQUENCY RESPONSE					
Bandwidth	V_{OUT} = 10Vp-p		14		kHz
Rise Fall Time, 10% to 90%	V_{OUT} = 10V Step		28		µs
Settling Time, 0.05%	V_{OUT} = 10V Step		160		µs
0.1%			80		µs
1%			70		µs
Overload Recovery	100%, Return to Linear Operation		50		µs
OUTPUT					
Voltage Output, High		(V_S) – 1.3	(V_S) – 1.15		V
Capacitive Load, Stable Operation			10		nF
Short-Circuit Current	V_S = 36V		15		mA
POWER SUPPLY					
Operating Voltage Range		+2.7		+36	V
Quiescent Current	Dark, V_{PIN3} = 0V		120	240	µA
	R_L = ∞, V_{OUT} = 10V		220		µA
TEMPERATURE RANGE					
Specification		0		+70	°C
Operating		0		+70	°C
Storage		–25		+85	°C
Thermal Resistance, θ_{JA}			100		°C/W

NOTES: (1) Deviation in percent of full scale from best-fit straight line. (2) Referred to Output. Includes all error sources.

PHOTODIODE SPECIFICATIONS

T_A = +25°C, V_S = +2.7V to +36V unless otherwise noted.

PARAMETER	CONDITIONS	Photodiode of OPT101P MIN	Photodiode of OPT101P TYP	Photodiode of OPT101P MAX	UNITS
Photodiode Area	(0.090 x 0.090in)		0.008		in^2
	(2.29 x 2.29mm)		5.2		mm^2
Current Responsivity	650nm		0.45		A/W
	650nm		865		$µA/W/cm^2$
Dark Current	V_{DIODE} = 7.5mV		2.5		pA
vs Temperature			Doubles every 7°C		
Capacitance			1200		pF

OP AMP SPECIFICATIONS

At T_A = +25°C, V_S = +2.7V to +36V, λ = 650nm, internal 1MΩ feedback resistor, and R_L = 10kΩ, unless otherwise noted.

PARAMETER	CONDITIONS	OPT101 Op Amp(1) MIN	OPT101 Op Amp(1) TYP	OPT101 Op Amp(1) MAX	UNITS
INPUT					
Offset Voltage			±0.5		mV
vs Temperature			±2.5		µV/°C
vs Power Supply			10		µV/V
Input Bias Current	(–) Input		165		pA
vs Temperature	(–) Input		Doubles every 10°C		
Input Impedance					
Differential			400 || 5		MΩ || pF
Common-Mode			250 || 35		GΩ || pF
Common-Mode Input Voltage Range	Linear Operation		0 to [(V_S) – 1]		V
Common-Mode Rejection			90		dB
OPEN-LOOP GAIN					
Open-loop Voltage Gain			90		dB
FREQUENCY RESPONSE					
Gain-Bandwidth Product(2)			2		MHz
Slew Rate			1		V/µs
Settling Time 1%			5.8		µs
0.1%			7.7		µs
0.05%			8.0		µs
OUTPUT					
Voltage Output, High		(V_S) – 1.3	(V_S) – 1.15		V
Short-Circuit Current	V_S = +36V		15		mA
POWER SUPPLY					
Operating Voltage Range		+2.7		+36	V
Quiescent Current	Dark, V_{PIN3} = 0V		120	240	µA
	R_L = ∞, V_{OUT} = 10V		220		µA

NOTES: (1) Op amp specifications provided for information and comparison only. (2) Stable gains ≥ 10V/V.

PACKAGE/ORDERING INFORMATION[1]

PRODUCT	PACKAGE-LEAD	PACKAGE DESIGNATOR	SPECIFIED TEMPERATURE RANGE	PACKAGE MARKING	ORDERING NUMBER	TRANSPORT MEDIA, QUANTITY
OPT101P	DIP-8	NTC	–25°C to +85°C	OPT101	OPT101P	Rail, 50
OPT101P-J	DIP-8, Surface Mount[2]	DTL	–25°C to +85°C	OPT101	OPT101P-J	Rail, 50

NOTES: (1) For the most current package and ordering information, see the Package Option Addendum at the end of this data sheet. (2) 8-pin DIP with J-formed leads for surface mounting.

PIN CONFIGURATIONS

Top View **DIP**

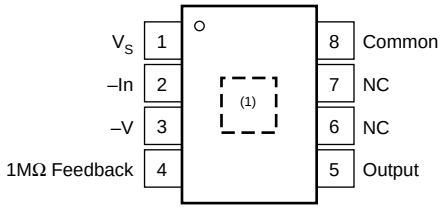

NOTE: (1) Photodiode location.

ABSOLUTE MAXIMUM RATINGS[1]

Supply Voltage (V_S to *"Common"* or pin 3)	0 to +36V
Output Short-Circuit (to ground)	Continuous
Operating Temperature	–25°C to +85°C
Storage Temperature	–25°C to +85°C
Junction Temperature	+85°C
Lead Temperature (soldering, 10s)	+300°C
(Vapor-Phase Soldering Not Recommended)	

NOTE: (1) Stresses above these ratings may cause permanent damage. Exposure to absolute maximum conditions for extended periods may degrade device reliability. These are stress ratings only, and functional operation of the device at these or any other conditions beyond those specified is not implied.

ELECTROSTATIC DISCHARGE SENSITIVITY

This integrated circuit can be damaged by ESD. Texas Instruments recommends that all integrated circuits be handled with appropriate precautions. Failure to observe proper handling and installation procedures can cause damage.

ESD damage can range from subtle performance degradation to complete device failure. Precision integrated circuits may be more susceptible to damage because very small parametric changes could cause the device not to meet its published specifications.

MOISTURE SENSITIVITY AND SOLDERING

Clear plastic does not contain the structural-enhancing fillers used in black plastic molding compound. As a result, clear plastic is more sensitive to environmental stress than black plastic. This can cause difficulties if devices have been stored in high humidity prior to soldering. The rapid heating during soldering can stress wire bonds and cause failures. Prior to soldering, it is recommended that plastic devices be baked-out at +85°C for 24 hours.

The fire-retardant fillers used in black plastic are not compatible with clear molding compound. The OPT101 plastic packages cannot meet flammability test, UL-94.

TYPICAL PERFORMANCE CURVES

At T_A = +25°C, V_S = +2.7V to +36V, λ = 650nm, internal 1MΩ feedback resistor, and R_L = 10kΩ, unless otherwise noted.

59

NORMALIZED SPECTRAL RESPONSIVITY

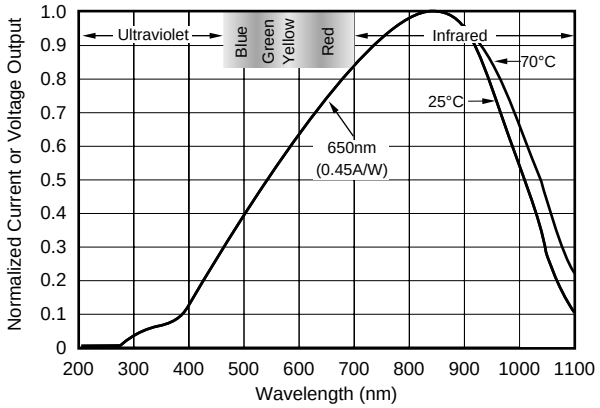

VOLTAGE RESPONSIVITY vs RADIANT POWER

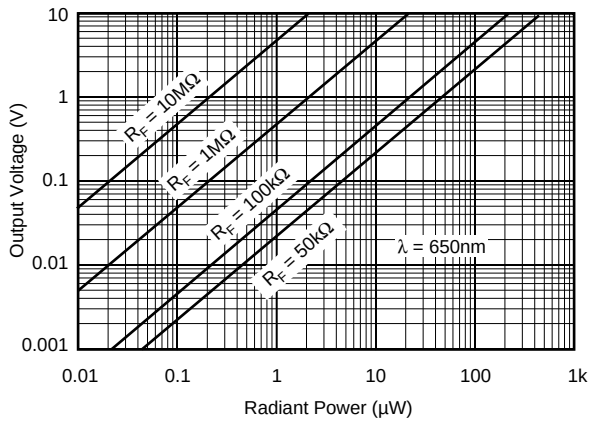

VOLTAGE RESPONSIVITY vs IRRADIANCE

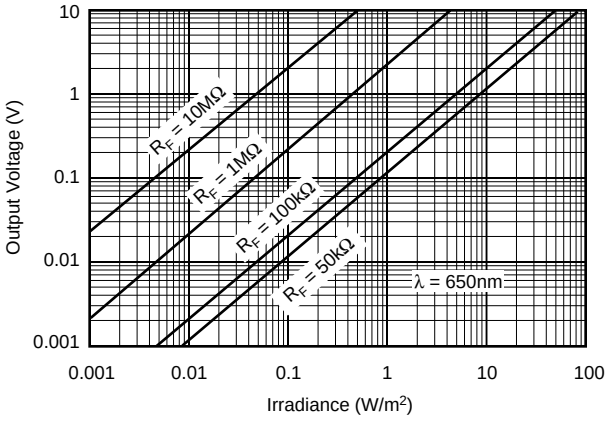

VOLTAGE RESPONSIVITY vs FREQUENCY

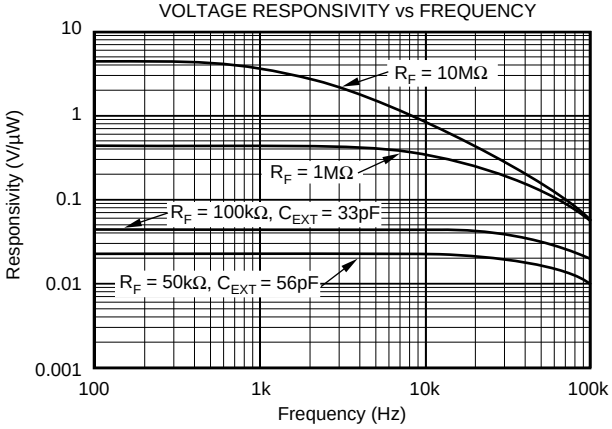

RESPONSE vs INCIDENT ANGLE

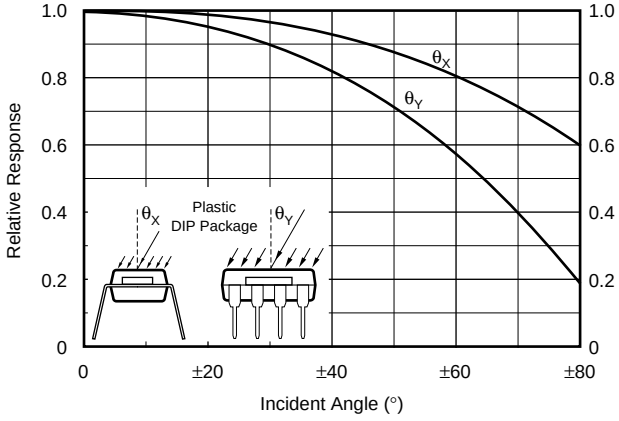

DARK V_{OUT} vs TEMPERATURE

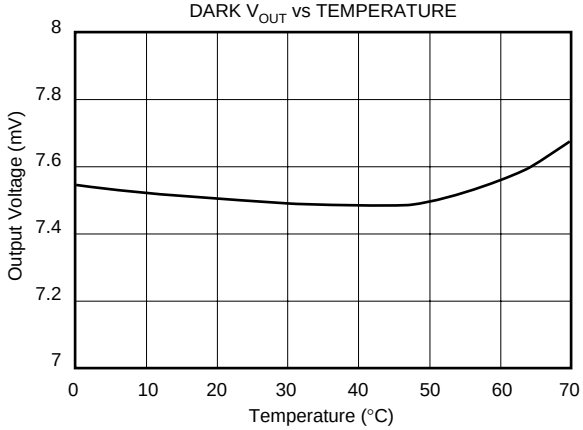

TYPICAL PERFORMANCE CURVES (Cont.)

At T_A = +25°C, V_S = +2.7V to +36V, λ = 650nm, internal 1MΩ feedback resistor, and R_L = 10kΩ, unless otherwise noted.

QUIESCENT CURRENT vs TEMPERATURE

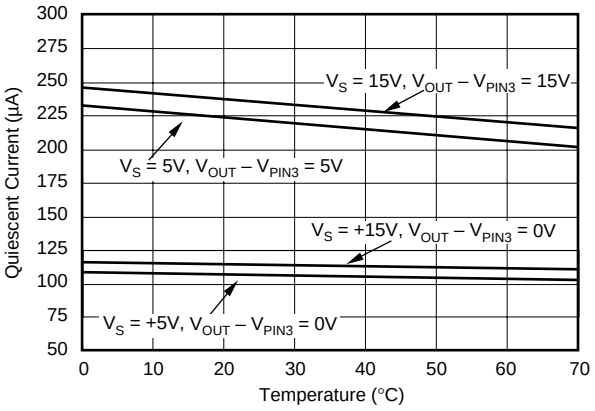

QUIESCENT CURRENT vs (V_{OUT} – V_{PIN3})

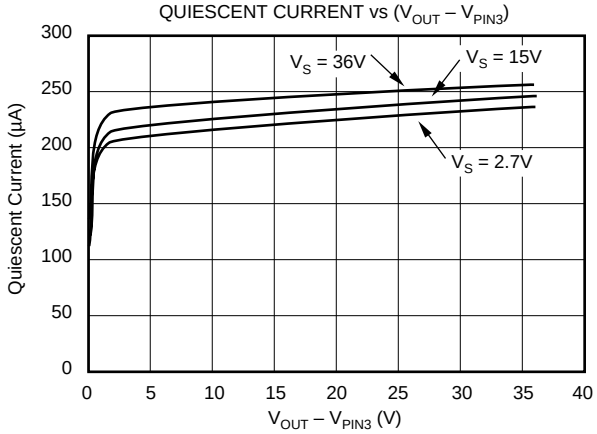

SHORT CIRCUIT CURRENT vs V_S

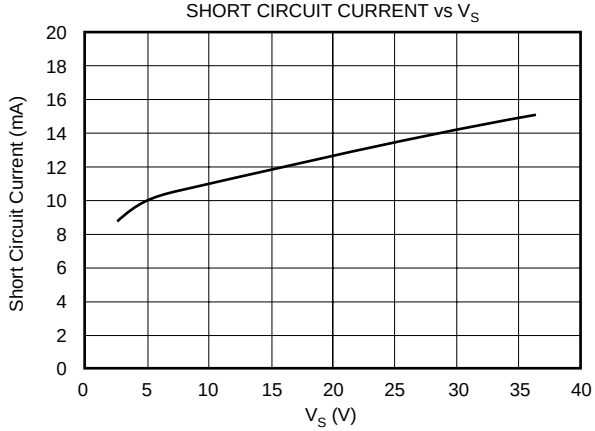

(I_{BIAS}-I_{DARK}) vs TEMPERATURE

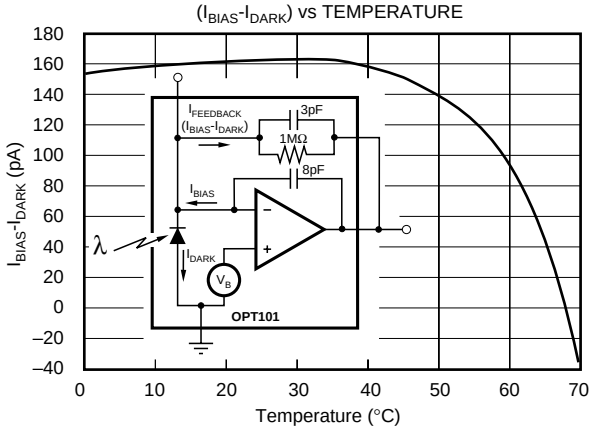

OUTPUT NOISE VOLTAGE vs
MEASUREMENT BANDWIDTH, V_S = +15, V_{OUT} – V_{PIN3} = 15V

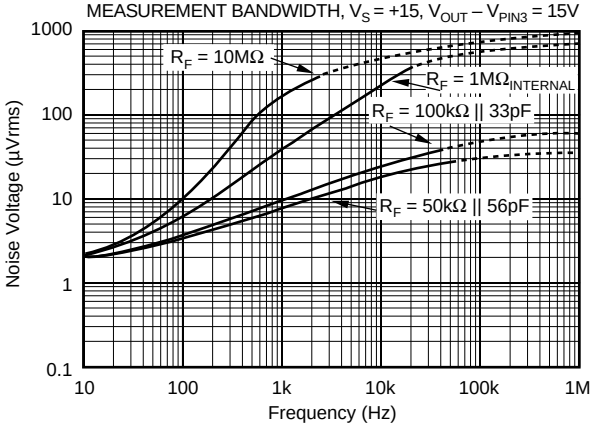

NOISE EFFECTIVE POWER vs
MEASUREMENT BANDWIDTH, V_S = +15, V_{OUT} – V_{PIN3} = 0

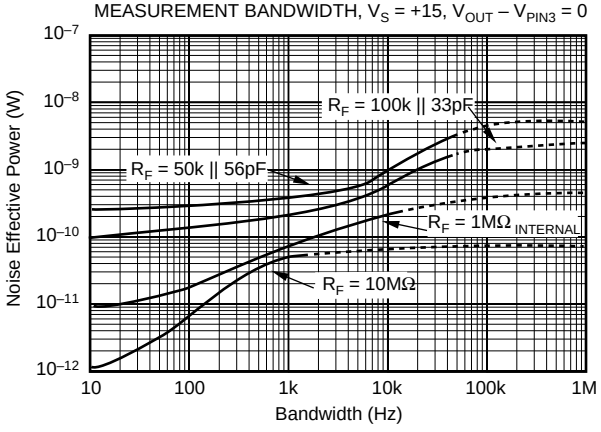

TYPICAL PERFORMANCE CURVES (Cont.)

At T_A = +25°C, V_S = +2.7V to +36V, λ = 650nm, internal 1MΩ feedback resistor, and R_L = 10kΩ, unless otherwise noted.

SMALL SIGNAL RESPONSE

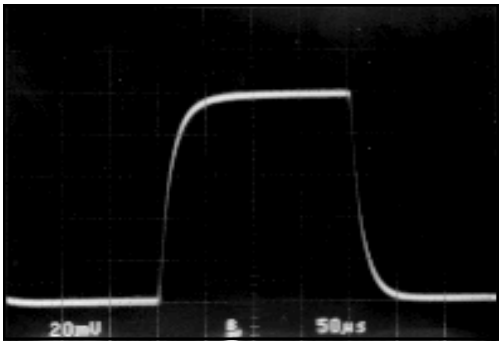

LARGE SIGNAL RESPONSE

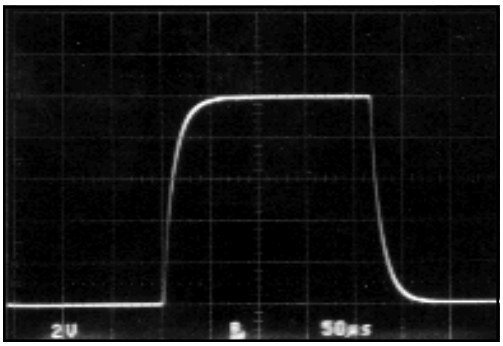

SMALL SIGNAL RESPONSE (C_{LOAD} = 10,000 pF)
(Pin 3 = 0V)

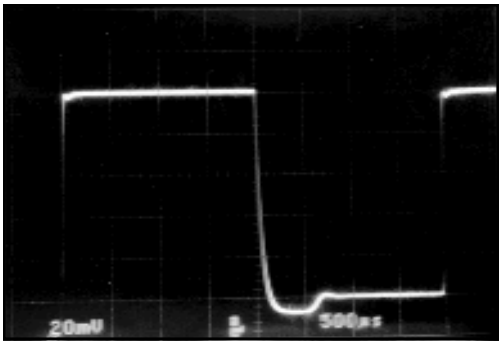

SMALL SIGNAL RESPONSE (C_{LOAD} = 10,000 pF)
(Pin 3 = –15V)

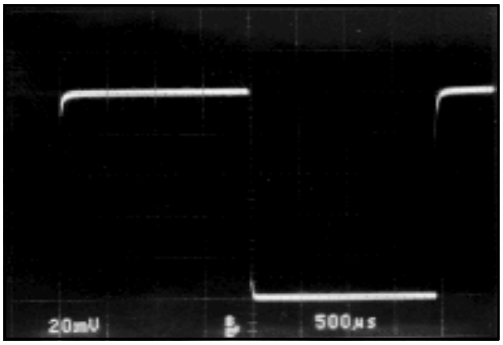

APPLICATIONS INFORMATION

Figure 1 shows the basic connections required to operate the OPT101. Applications with high-impedance power supplies may require decoupling capacitors located close to the device pins as shown. Output is 7.5mV dc with no light and increases with increasing illumination.

Photodiode current, I_D, is proportional to the radiant power, or flux, (in watts) falling on the photodiode. At a wavelength of 650nm (visible red) the photodiode Responsivity, R_I, is approximately 0.45A/W. Responsivity at other wavelengths is shown in the typical performance curve “Responsivity vs Wavelength.”

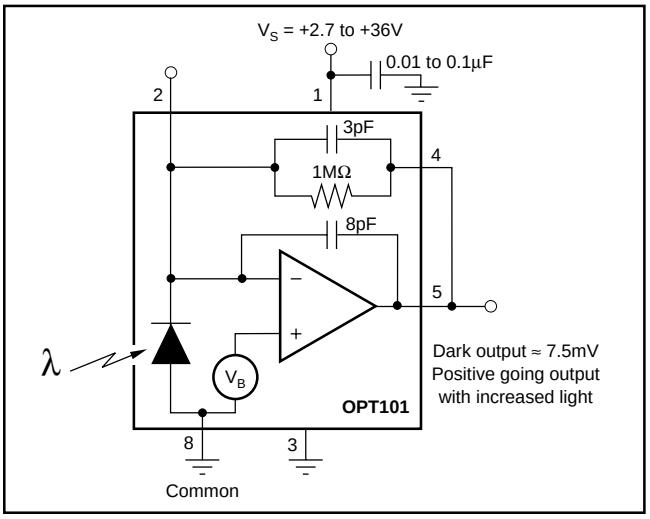

FIGURE 1. Basic Circuit Connections.

The typical performance curve “Output Voltage vs Radiant Power” shows the response throughout a wide range of radiant power. The response curve “Output Voltage vs Irradiance” is based on the photodiode area of 5.2mm^2.

The OPT101’s voltage output is the product of the photodiode current times the feedback resistor, ($I_D R_F$), plus a pedestal voltage, V_B, of approximately 7.5mV introduced for single supply operation. The internal feedback resistor is laser trimmed to 1MΩ. Using this resistor, the output voltage responsivity, R_V, is approximately 0.45V/µW at 650nm wavelength. Figure 1 shows the basic circuit connections for the OPT101 operating with a single power supply and using the internal 1MΩ feedback resistor for a response of 0.45V/µW at 650nm. Pin 3 is connected to common in this configuration.

CAPACITIVE LOADING

The OPT101 is capable of driving load capacitances of 10nF without instability. However, dynamic performance with capacitive loads can be improved by applying a negative bias voltage to Pin 3 (shown in Figure 2). This negative power supply voltage allows the output to go negative in response to the reactive effect of a capacitive load. An internal JFET connected between pin 5 (output) and pin 3 allows the output to sink current. This current sink capability can also be useful when driving the capacitive inputs of some analog-to-digital converters which require the signal source to sink currents up to approximately 100µA. The benefits of this current sink are shown in the typical performance curves “Small Signal Response (C_{LOAD} = 10,000pF)” which compare operation with pin 3 grounded and connected to –15V.

Due to the architecture of this output stage current sink, there is a slight increase in operating current when there is a voltage between pin 3 and the output. Depending on the magnitude of this voltage, the quiescent current will increase by approximately 100µA as shown in the typical performance curve "Quiescent Current vs ($V_{OUT} - V_{PIN3}$)".

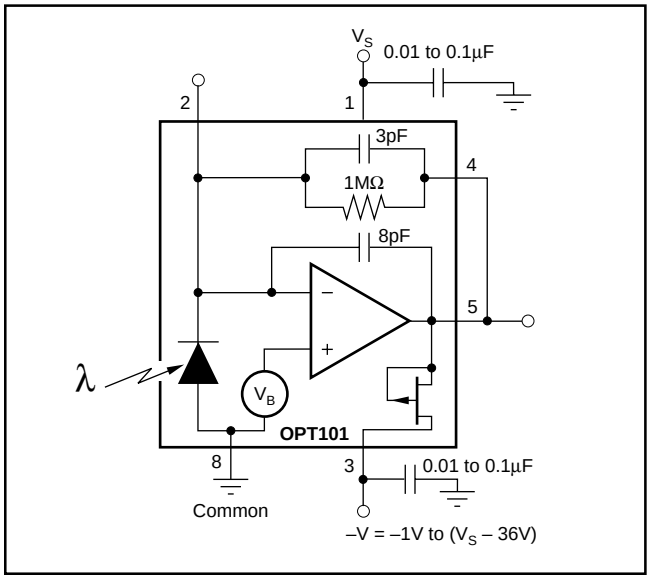

FIGURE 2. Bipolar Power Supply Circuit Connections.

NOISE PERFORMANCE

Noise performance of the OPT101 is determined by the op amp characteristics, feedback components and photodiode capacitance. The typical performance curve “Output Noise Voltage vs Measurement Bandwidth” shows how the noise varies with R_F and measured bandwidth (0.1Hz to the indicated frequency), when the output voltage minus the voltage on pin 3 is greater than approximately 50mV. Below this level, the output stage is powered down, and the effective bandwidth is decreased. This reduces the noise to approximately 1/3 the nominal noise value of 300µVrms, or 100µVrms. This enables a low level signal to be resolved.

Noise can be reduced by filtering the output with a cutoff frequency equal to the signal bandwidth. This will improve signal-to-noise ratio. Also, output noise increases in proportion to the square root of the feedback resistance, while responsivity increases linearly with feedback resistance. Best signal-to-noise ratio is achieved with large feedback resistance. This comes with the trade-off of decreased bandwidth.

The noise performance of the photodetector is sometimes characterized by *Noise Effective Power* (NEP). This is the radiant power that would produce an output signal equal to the noise level. NEP has the units of radiant power (watts), or Watts/$\sqrt{\text{Hz}}$ to convey spectral information about the noise. The typical performance curve “Noise Effective Power” vs Measurement Bandwidth" illustrates the NEP for the OPT101.

DARK ERRORS

The dark errors in the specification table include all sources. The dominant source of dark output voltage is the "pedestal" voltage applied to the non-inverting input of the op amp. This voltage is introduced to provide linear operation in the absence of light falling on the photodiode. Photodiode dark current is approximately 2.5pA and contributes virtually no offset error at room temperature. The bias current of the op amp's summing junction (– input) is approximately 165pA. The dark current will be subtracted from the amplifier's bias current, and this residual current will flow through the feedback resistor creating an offset. The effects of temperature on this difference current can be seen in the typical performance curve "(I_{BIAS} – I_{DARK}) vs Temperature." The dark output voltage can be trimmed to zero with the optional circuit shown in Figure 3. A low impedance offset driver (op amp) should be used to drive pin 8 because this node has signal-dependent currents.

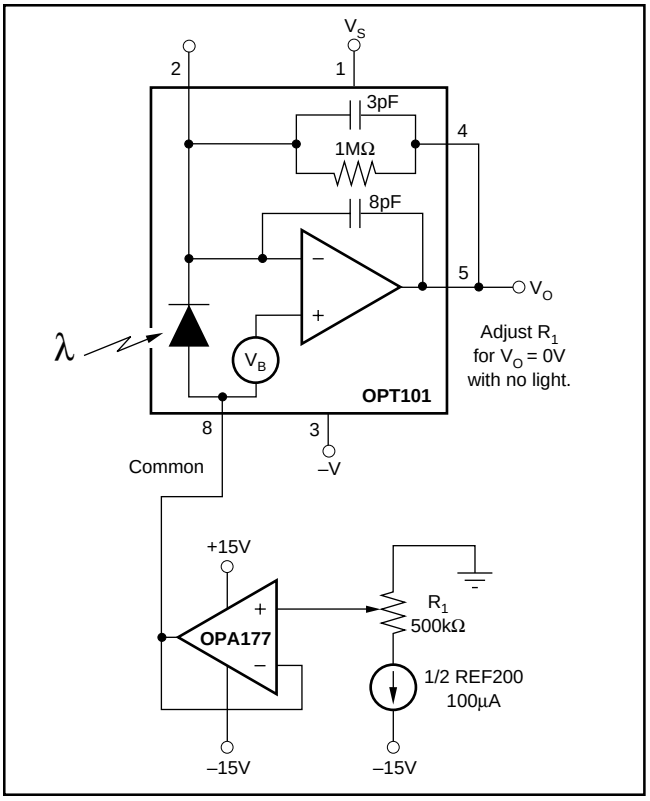

FIGURE 3. Dark Error (Offset) Adjustment Circuit.

CHANGING RESPONSIVITY

An external resistor, R_{EXT}, can be connected to set a different voltage responsivity. To increase the responsivity, this resistor can be placed in series with the internal 1MΩ (Figure 4a), or the external resistor can replace the internal resistor by not connecting pin 4 (Figure 4b). The second configuration also allows the circuit gain to be reduced below 10^6V/A by using external resistors of less than 1MΩ.

Figure 4 includes tables showing the responsivity and bandwidth. For values of R_F less than 1MΩ, an external capacitor, C_{EXT} should be connected in parallel with R_F. This capacitor eliminates gain peaking and prevents instability. The value of C_{EXT} can be determined from the table in Figure 4. Values of R_F, other than shown in the table, can be interpolated.

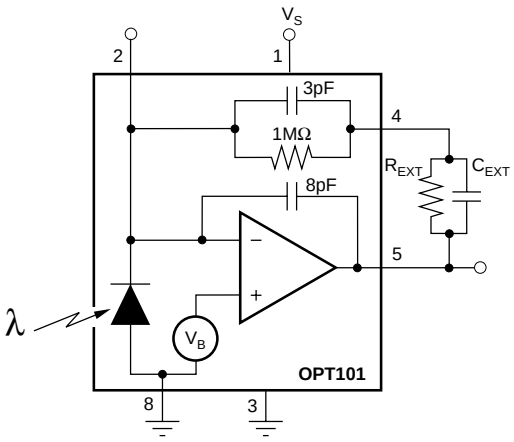

(a)-Series R_{EXT}

R_{EXT} (MΩ)	C_{EXT} (pF)	DC Gain (x10^6V/A)	Bandwidth (kHz)
1	50	2	8
2	25	3	6
5	10	6	2.5
10	5	11	1.3
50	—	51	0.33

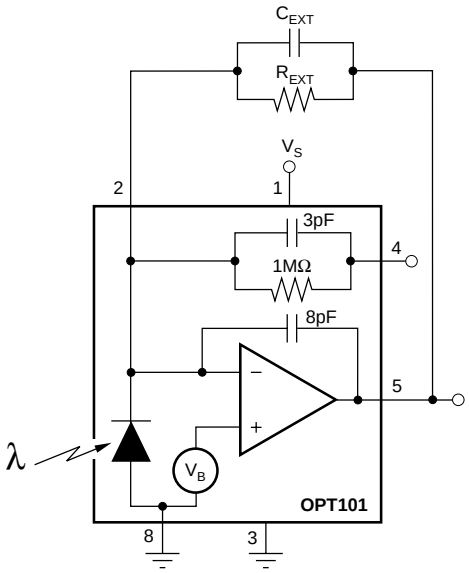

(b)-External Feedback

R_{EXT} (MΩ)	C_{EXT} (pF)	DC Gain (x10^6V/A)	Bandwidth (kHz)
0.05(1)	56	0.05	58
0.1(1)	33	0.1	44
1	—	1	23
2	—	2	9.4
5	—	5	3.6
10	—	10	1.8
50	—	50	0.34

Note: (1) May require 1kΩ in series with pin 5 when driving large capacitances.

FIGURE 4. Changing Responsivity with External Resistor.

Applications using a feedback resistor significantly larger than the internal 1MΩ resistor may require special consideration. Input bias current of the op amp and dark current of the photodiode increase significantly at higher temperatures. This increase combined with the higher gain (R_F > 1MΩ) can cause the op amp output to be driven to ground at high temperatures. Such applications may require a positive bias voltage applied to pin 8 to ensure that the op amp output remains in the linear operating region when the photodiode is not exposed to light. Alternatively, a dual power supply can be used. The output may be negative when sensing dark conditions.

LIGHT SOURCE POSITIONING

The OPT101 is tested with a light source that uniformly illuminates the full area of the integrated circuit, including the op amp. Although IC amplifiers are light-sensitive to some degree, the OPT101 op amp circuitry is designed to minimize this effect. Sensitive junctions are shielded with metal, and the photodiode area is very large relative to the op amp input circuitry.

If your light source is focused to a small area, be sure that it is properly aimed to fall on the photodiode. A narrowly focused beam falling on only the photodiode will provide improved settling times compared to a source that uniformly illuminates the full area of the die. If a narrowly focused light source were to miss the photodiode area and fall only on the op amp circuitry, the OPT101 would not perform properly. The large 0.09" x 0.09" (2.29mm x 2.29mm) photodiode area allows easy positioning of narrowly focused light sources. The photodiode area is easily visible, as it appears very dark compared to the surrounding active circuitry.

The incident angle of the light source also effects the apparent sensitivity in uniform irradiance. For small incident angles, the loss in sensitivity is simply due to the smaller effective light gathering area of the photodiode (proportional to the cosine of the angle). At a greater incident angle, light is diffracted and scattered by the package. These effects are shown in the typical performance curve “Responsivity vs Incident Angle.”

DYNAMIC RESPONSE

Using the internal 1MΩ resistor, the dynamic response of the photodiode/op amp combination can be modeled as a simple R • C circuit with a –3dB cutoff frequency of approximately 14kHz. The R and C values are 1MΩ and 11pF respectively. By using external resistors, with less than 3pF parasitic capacitance, the frequency response can be improved. An external 1MΩ resistor used in the configuration shown in Figure 4b will create a 23kHz bandwidth with the same 10^6V/A dc transimpedance gain. This yields a rise time of approximately 15µs (10% to 90%). Dynamic response is not limited by op amp slew rate. This is demonstrated by the dynamic response oscilloscope photographs showing virtually identical large-signal and small-signal response.

Dynamic response will vary with feedback resistor value as shown in the typical performance curve “Responsivity vs Frequency.” Rise time (10% to 90%) will vary according to the –3dB bandwidth produced by a given feedback resistor value:

$$t_r = \frac{0.35}{f_C}$$

where:

t_r is the rise time (10% to 90%)

f_C is the –3dB bandwidth

LINEARITY PERFORMANCE

The photodiode is operated in the photoconductive mode so the current output of the photodiode is very linear with radiant power throughout a wide range. Nonlinearity remains below approximately 0.05% up to 100µA photodiode current. The photodiode can produce output currents of 1mA or greater with high radiant power, but nonlinearity increases to several percent in this region.

This very linear performance at high radiant power assumes that the full photodiode area is uniformly illuminated. If the light source is focused to a small area of the photodiode, nonlinearity will occur at lower radiant power.

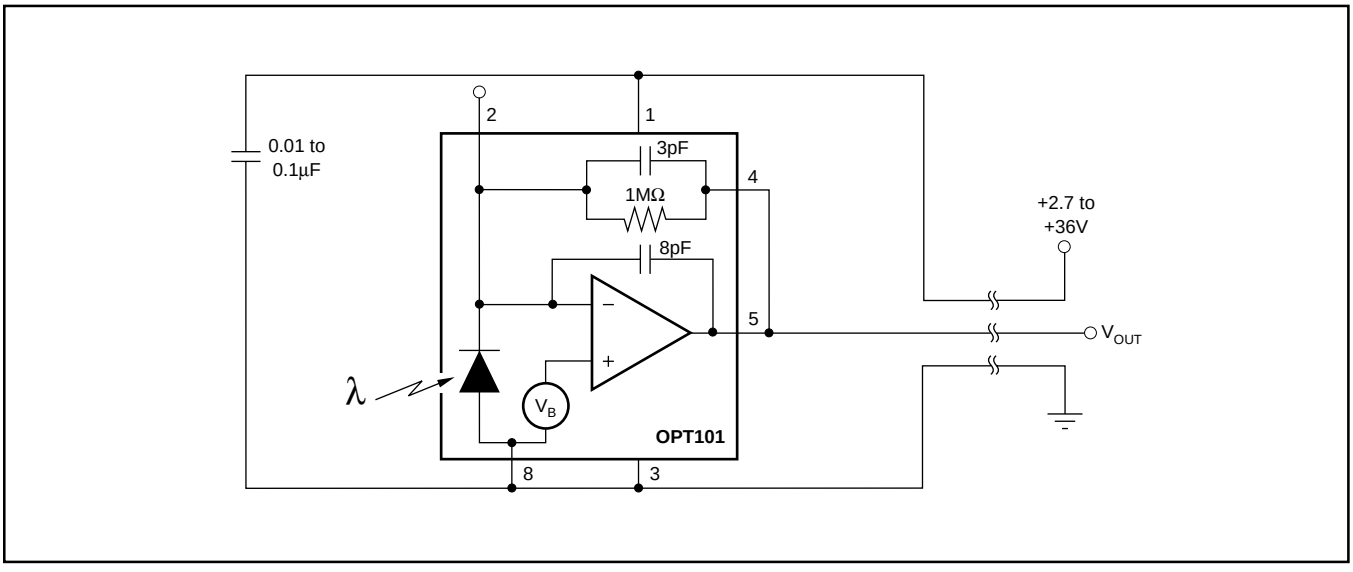

FIGURE 5. Three-Wire Remote Light Measurement.

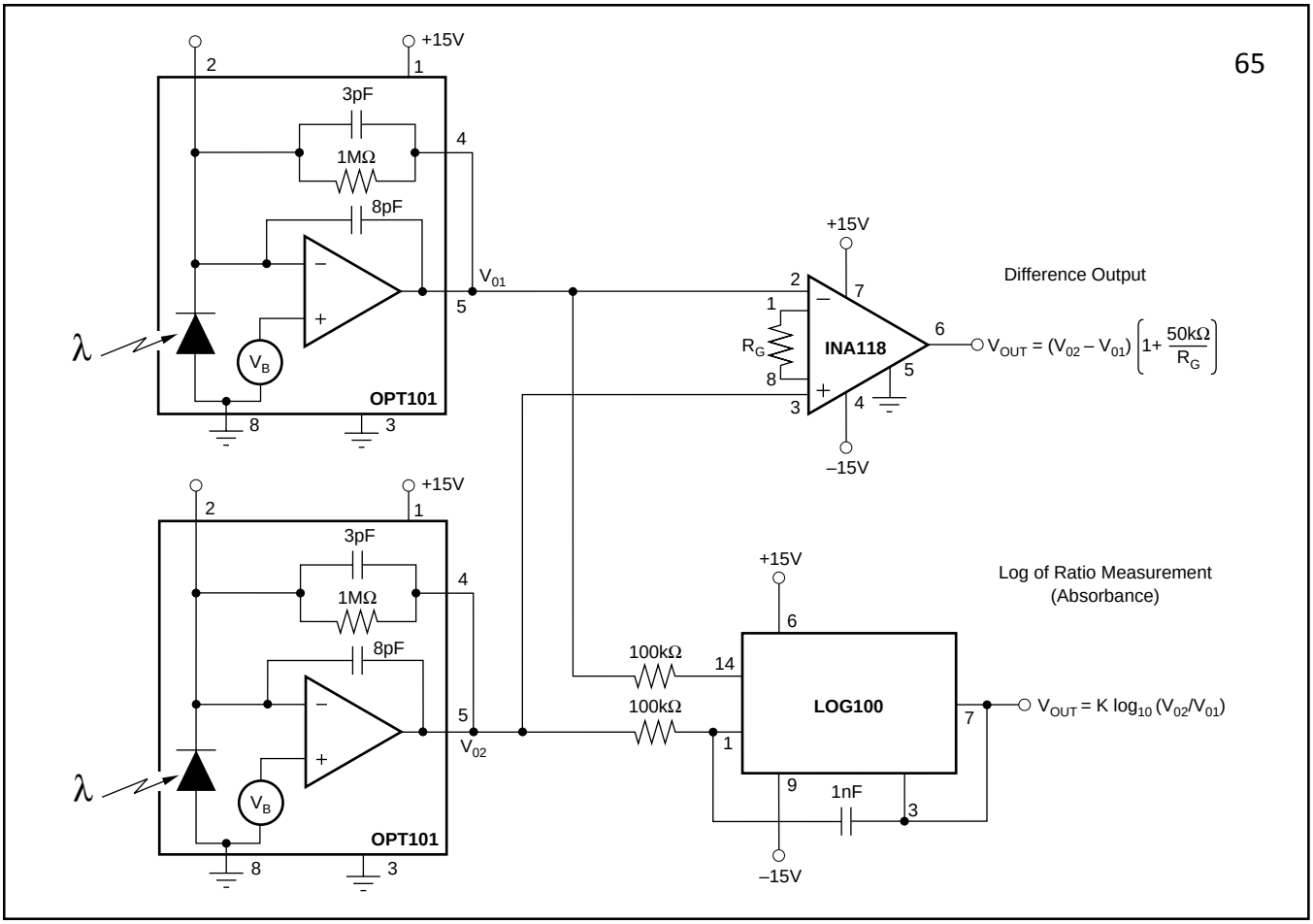

FIGURE 6. Differential Light Measurement.

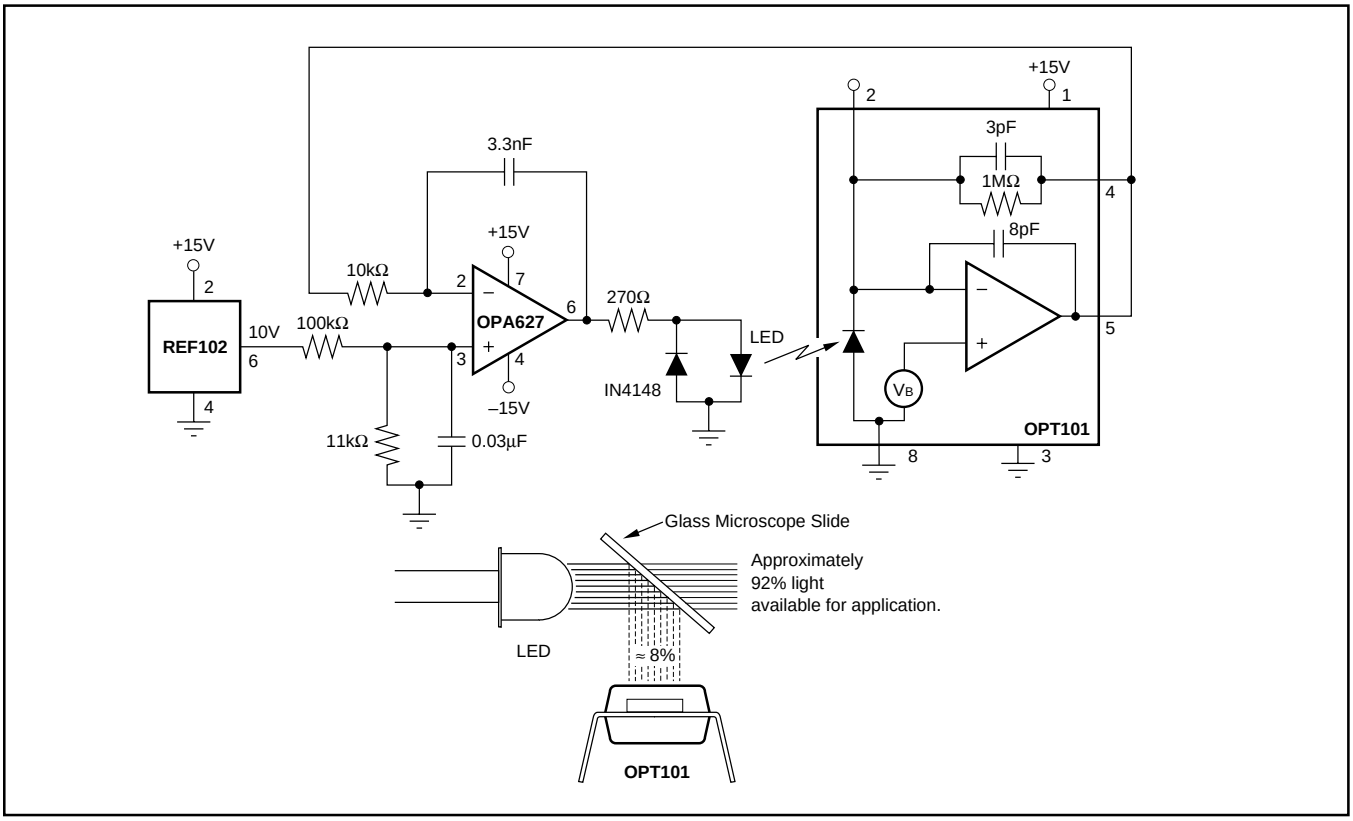

FIGURE 7. LED Output Regulation Circuit.

PACKAGING INFORMATION

Orderable Device	Status (1)	Package Type	Package Drawing	Pins	Package Qty	Eco Plan (2)	Lead/Ball Finish	MSL Peak Temp (3)
OPT101P	ACTIVE	PDIP	NTC	8	50	Green (RoHS & no Sb/Br)	CU NIPDAU	N / A for Pkg Type
OPT101P-J	ACTIVE	SOP	DTL	8	50	Green (RoHS & no Sb/Br)	CU NIPDAU	Level-4-250C-72 HR
OPT101P-JG4	ACTIVE	SOP	DTL	8	50	Green (RoHS & no Sb/Br)	CU NIPDAU	Level-4-250C-72 HR
OPT101PG4	ACTIVE	PDIP	NTC	8	50	Green (RoHS & no Sb/Br)	CU NIPDAU	N / A for Pkg Type

(1) The marketing status values are defined as follows:
ACTIVE: Product device recommended for new designs.
LIFEBUY: TI has announced that the device will be discontinued, and a lifetime-buy period is in effect.
NRND: Not recommended for new designs. Device is in production to support existing customers, but TI does not recommend using this part in a new design.
PREVIEW: Device has been announced but is not in production. Samples may or may not be available.
OBSOLETE: TI has discontinued the production of the device.

(2) Eco Plan - The planned eco-friendly classification: Pb-Free (RoHS), Pb-Free (RoHS Exempt), or Green (RoHS & no Sb/Br) - please check http://www.ti.com/productcontent for the latest availability information and additional product content details.
TBD: The Pb-Free/Green conversion plan has not been defined.
Pb-Free (RoHS): TI's terms "Lead-Free" or "Pb-Free" mean semiconductor products that are compatible with the current RoHS requirements for all 6 substances, including the requirement that lead not exceed 0.1% by weight in homogeneous materials. Where designed to be soldered at high temperatures, TI Pb-Free products are suitable for use in specified lead-free processes.
Pb-Free (RoHS Exempt): This component has a RoHS exemption for either 1) lead-based flip-chip solder bumps used between the die and package, or 2) lead-based die adhesive used between the die and leadframe. The component is otherwise considered Pb-Free (RoHS compatible) as defined above.
Green (RoHS & no Sb/Br): TI defines "Green" to mean Pb-Free (RoHS compatible), and free of Bromine (Br) and Antimony (Sb) based flame retardants (Br or Sb do not exceed 0.1% by weight in homogeneous material)

(3) MSL, Peak Temp. -- The Moisture Sensitivity Level rating according to the JEDEC industry standard classifications, and peak solder temperature.

Important Information and Disclaimer: The information provided on this page represents TI's knowledge and belief as of the date that it is provided. TI bases its knowledge and belief on information provided by third parties, and makes no representation or warranty as to the accuracy of such information. Efforts are underway to better integrate information from third parties. TI has taken and continues to take reasonable steps to provide representative and accurate information but may not have conducted destructive testing or chemical analysis on incoming materials and chemicals. TI and TI suppliers consider certain information to be proprietary, and thus CAS numbers and other limited information may not be available for release.

In no event shall TI's liability arising out of such information exceed the total purchase price of the TI part(s) at issue in this document sold by TI to Customer on an annual basis.

DTL (R–PDSO–U8) PLASTIC SMALL–OUTLINE

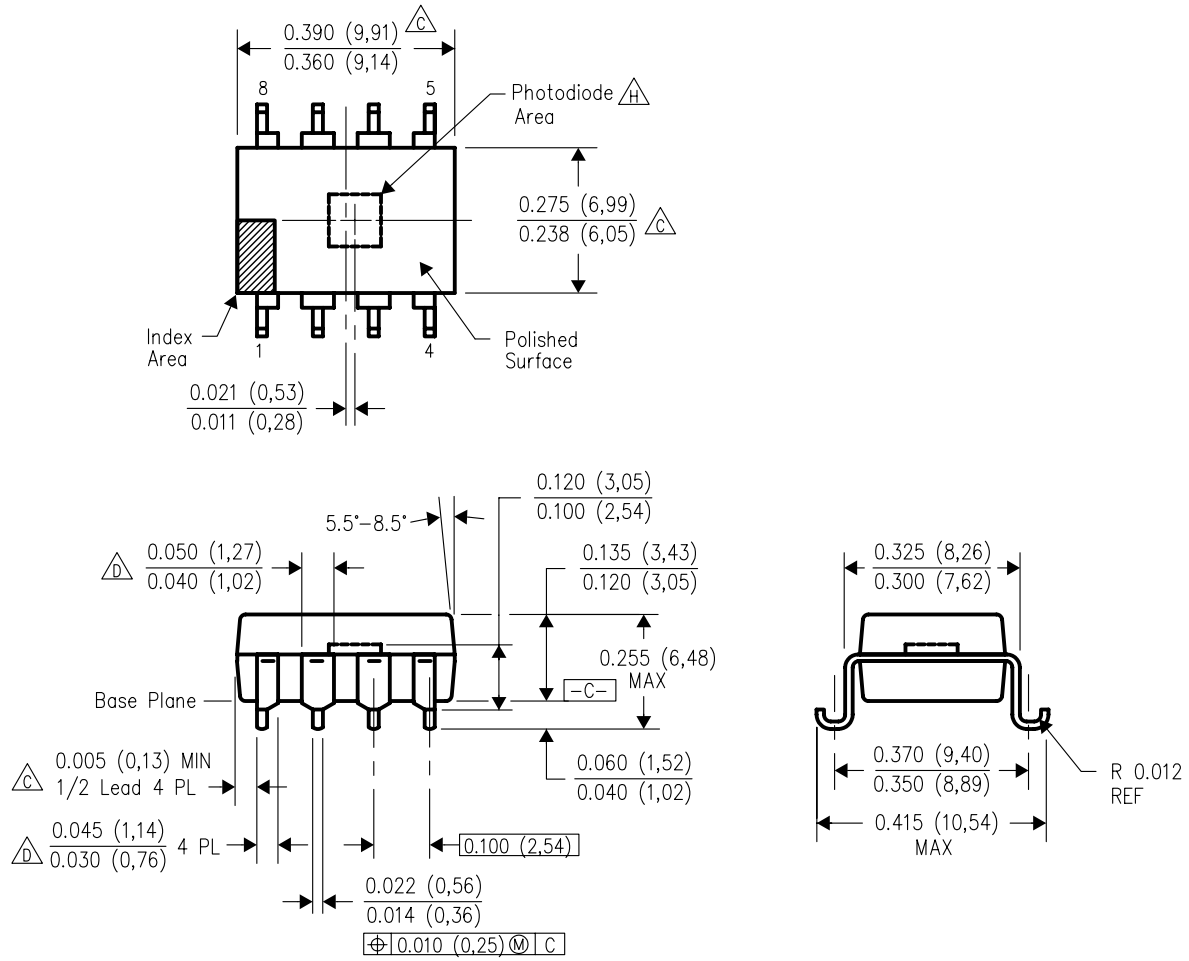

4202637/C 11/03

NOTES:
A. All linear dimensions are in inches (millimeters).
B. This drawing is subject to change without notice.
C. Dimensions do not include mold flash or protrusions Mold flash or protrusions shall not exceed 0.010 (0,25).
D. Maximum dimensions do not include dambar protrusions. Dambar protrusions shall not exceed 0.010 (0,25).
E. Distance between leads including dambar protrusions to be 0.005 (0,13) minumum.
F. A visual index feature must be located within the cross–hatched area.
G. For automatic insertion, any raised irregularity on the top surface (step, mesa, etc.) shall be symmetrical about the lateral and longitudinal package centerlines.
H. Center of photodiode must be within 0.010 (0,25) of center of photodiode area.

NTC (R-PDIP-T8) **PLASTIC DUAL-IN-LINE**

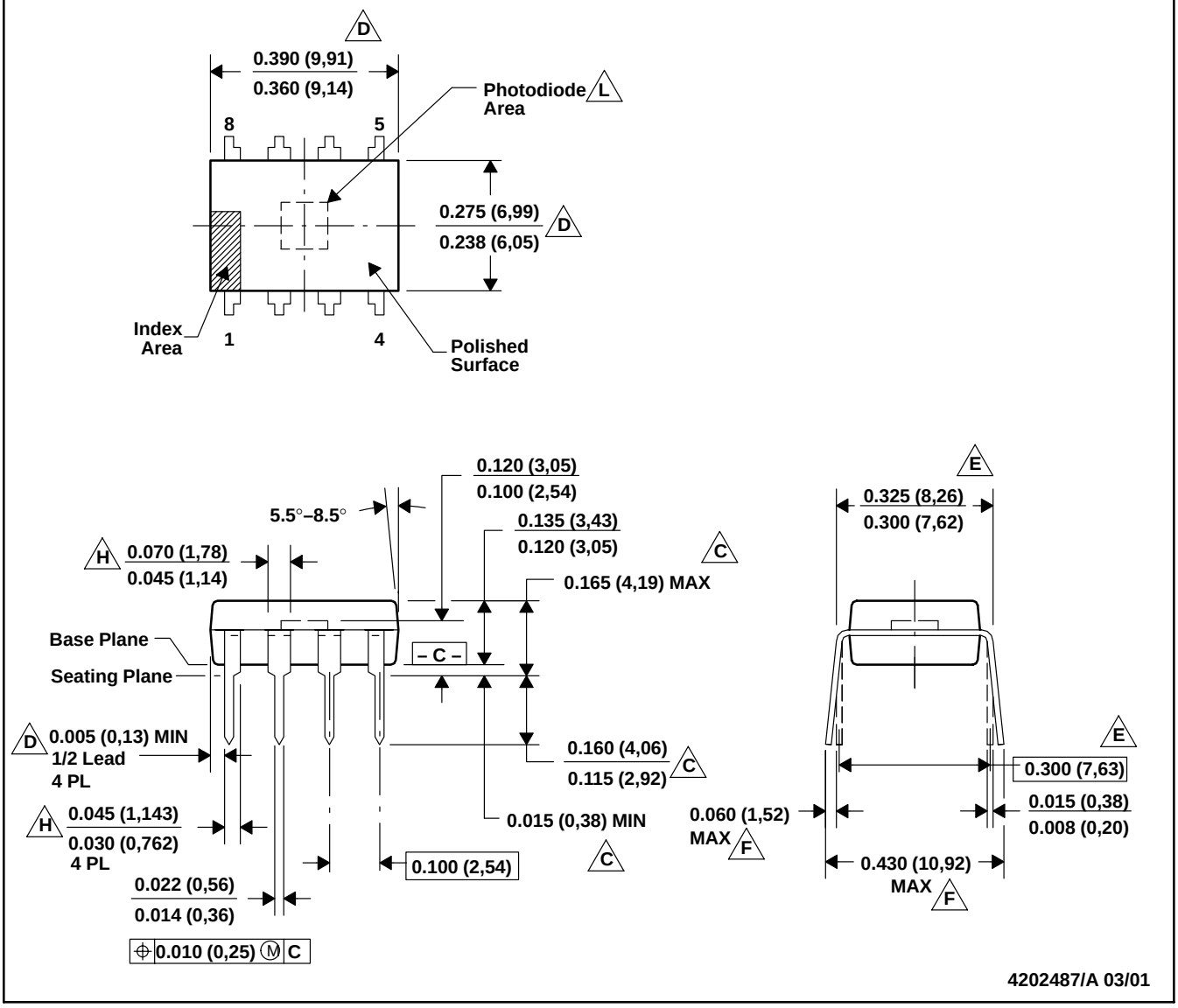

NOTES:
A. All linear dimensions are in inches (millimeters).
B. This drawing is subject to change without notice.
C. Dimensions are measured with the package seated in JEDEC seating plane gauge GS-3.
D. Dimensions do not include mold flash or protrusions. Mold flash or protrusions shall not exceed 0.010 (0,25).
E. Dimensions measured with the leads constrained to be perpendicular to Datum C.
F. Dimensions are measured at the lead tips with the leads unconstrained.
G. Pointed or rounded lead tips are preferred to ease insertion.
H. Maximum dimensions do not include dambar protrusions. Dambar protrusions shall not exceed 0.010 (0,25).
I. Distance between leads including dambar protrusions to be 0.005 (0,13) minumum.
J. A visual index feature must be located within the cross–hatched area.
K. For automatic insertion, any raised irregularity on the top surface (step, mesa, etc.) shall be symmetrical about the lateral and longitudinal package centerlines.
L. Center of photodiode must be within 0.010 (0,25) of center of photodiode area

IMPORTANT NOTICE

Texas Instruments Incorporated and its subsidiaries (TI) reserve the right to make corrections, modifications, enhancements, improvements, and other changes to its products and services at any time and to discontinue any product or service without notice. Customers should obtain the latest relevant information before placing orders and should verify that such information is current and complete. All products are sold subject to TI's terms and conditions of sale supplied at the time of order acknowledgment.

TI warrants performance of its hardware products to the specifications applicable at the time of sale in accordance with TI's standard warranty. Testing and other quality control techniques are used to the extent TI deems necessary to support this warranty. Except where mandated by government requirements, testing of all parameters of each product is not necessarily performed.

TI assumes no liability for applications assistance or customer product design. Customers are responsible for their products and applications using TI components. To minimize the risks associated with customer products and applications, customers should provide adequate design and operating safeguards.

TI does not warrant or represent that any license, either express or implied, is granted under any TI patent right, copyright, mask work right, or other TI intellectual property right relating to any combination, machine, or process in which TI products or services are used. Information published by TI regarding third-party products or services does not constitute a license from TI to use such products or services or a warranty or endorsement thereof. Use of such information may require a license from a third party under the patents or other intellectual property of the third party, or a license from TI under the patents or other intellectual property of TI.

Reproduction of TI information in TI data books or data sheets is permissible only if reproduction is without alteration and is accompanied by all associated warranties, conditions, limitations, and notices. Reproduction of this information with alteration is an unfair and deceptive business practice. TI is not responsible or liable for such altered documentation. Information of third parties may be subject to additional restrictions.

Resale of TI products or services with statements different from or beyond the parameters stated by TI for that product or service voids all express and any implied warranties for the associated TI product or service and is an unfair and deceptive business practice. TI is not responsible or liable for any such statements.

TI products are not authorized for use in safety-critical applications (such as life support) where a failure of the TI product would reasonably be expected to cause severe personal injury or death, unless officers of the parties have executed an agreement specifically governing such use. Buyers represent that they have all necessary expertise in the safety and regulatory ramifications of their applications, and acknowledge and agree that they are solely responsible for all legal, regulatory and safety-related requirements concerning their products and any use of TI products in such safety-critical applications, notwithstanding any applications-related information or support that may be provided by TI. Further, Buyers must fully indemnify TI and its representatives against any damages arising out of the use of TI products in such safety-critical applications.

TI products are neither designed nor intended for use in military/aerospace applications or environments unless the TI products are specifically designated by TI as military-grade or "enhanced plastic." Only products designated by TI as military-grade meet military specifications. Buyers acknowledge and agree that any such use of TI products which TI has not designated as military-grade is solely at the Buyer's risk, and that they are solely responsible for compliance with all legal and regulatory requirements in connection with such use.

TI products are neither designed nor intended for use in automotive applications or environments unless the specific TI products are designated by TI as compliant with ISO/TS 16949 requirements. Buyers acknowledge and agree that, if they use any non-designated products in automotive applications, TI will not be responsible for any failure to meet such requirements.

Following are URLs where you can obtain information on other Texas Instruments products and application solutions:

Products		**Applications**	
Amplifiers	amplifier.ti.com	Audio	www.ti.com/audio
Data Converters	dataconverter.ti.com	Automotive	www.ti.com/automotive
DLP® Products	www.dlp.com	Broadband	www.ti.com/broadband
DSP	dsp.ti.com	Digital Control	www.ti.com/digitalcontrol
Clocks and Timers	www.ti.com/clocks	Medical	www.ti.com/medical
Interface	interface.ti.com	Military	www.ti.com/military
Logic	logic.ti.com	Optical Networking	www.ti.com/opticalnetwork
Power Mgmt	power.ti.com	Security	www.ti.com/security
Microcontrollers	microcontroller.ti.com	Telephony	www.ti.com/telephony
RFID	www.ti-rfid.com	Video & Imaging	www.ti.com/video
RF/IF and ZigBee® Solutions	www.ti.com/lprf	Wireless	www.ti.com/wireless

Mailing Address: Texas Instruments, Post Office Box 655303, Dallas, Texas 75265
Copyright © 2009, Texas Instruments Incorporated

APPENDIX - B: CIRCUIT CONNECTIONS FOR ADAPTER CIRCUIT

Connector on PCB

Pin No.	Description
1	Det. 1
2	Det. 3
3	(+5V)
4	(+5V)
5	LED 805
6	LED2 850
7	LED1 850
8	LED1 730
9	LED2 730
10	LED 805
11	GND
12	GND
13	Det. 2
14	Det. 4
15	+V (LED PWR)
16	+V (LED PWR)
17	Det (out)
18	(+5V)
19	Det (out)
20	Det (out)
21	Det (out)
22	Det (out)
23	GND
24	Det (out)
25	(+5V)
26	GND
27	Det 10
28	Det 8
29	Det 6
30	+V (LED PWR)
31	+V (LED PWR)
32	LED 805
33	LED3 730
34	LED4 730
35	LED4 850
36	LED3 850
37	LED 805
38	Det 5
39	Det 7
40	Det 9

Probe (A)			
Pin No.	**Description**	**Pin No. on PCB**	**Notes**
1	LED PWR	15	
2	LED 730	7	LED1 730
3	LED 850	8	LED1 850
4	(+5V)	3	
5	GND	11	
6	Det. 1	1	Det. 1
7	Det. 2	13	Det. 2
8	Det. 3	3	Det. 3

Probe (B)			
Pin No.	**Description**	**Pin No. on PCB**	**Notes**
1	LED PWR	30	
2	LED 730	34	LED4 730
3	LED 850	35	LED4 850
4	(+5V)	25	
5	GND	12	
6	Det. 1	28	Det. 8
7	Det. 2	40	Det. 9
8	Det. 3	27	Det. 10

Probe (C)			
Pin No.	**Description**	**Pin No. on PCB**	**Notes**
1	LED PWR	31	
2	LED 730	33	LED3 730
3	LED 850	36	LED3 850
4	(+5V)	18	
5	GND	23	
6	Det. 1	38	Det. 5
7	Det. 2	29	Det. 6